### 4.4.2. Per-unit approach during alternate loads

The previously defined steady-state base values were proposed taking into account that fuel cells generate dc electric power, and that their theoretical operation point is a fixed point. However, fuel cells are able to admit an ac component superimposed to its dc operation point, which may be due to the particularities of the load or to the influence of the power converter to which it is connected [84]. The frequency and amplitude of this ac component can influence the fuel cell output power and life. An increase of this ac component will reduce the output power and a high load frequency can provoke concentration voltage drops due to the inability of reactants to reach the catalyst layers at the required speed.

For these situations it may be interesting to model the fuel cell taking into account the influence of frequency on the fuel cell impedance. This dependency is reflected on the EIS tests carried out. The fuel cell impedance varies from capacitive, to resistive and inductive behavior depending on the frequency of the load ac component.

To take into account these ac components on a per-unit system it is necessary to define a base frequency. Even though Choi [84] also defined a per-unit system he did not take into account the influence of an ac load on the per-unit system, even though he defined a dc and ac equivalent circuit. Hence, a criterion for the selection of the base frequency should be established. Studying the Nyquist plot, there are two singular candidate points to be considered. The first one is the cut-off frequency for $R_1C_1$, defined as seen in (4.14), and shown in Fig. 4.21.

$$f_{c1} = \frac{1}{R_1 C_1} \tag{4.14}$$

The second possible point is the resonance frequency, pointed out in Fig. 4.21 as the frequency at which the capacitive and inductive impedances cancel each other, and therefore the fuel cell impedance becomes purely resistive. The choice of the resonance frequency as the base frequency has a relevant advantage compared to the cut-off frequency, which is the simple identification in the Nyquist plot where Im[Z(w)] = 0, or in the Bode plot, where $\omega = 0$. Moreover, there is a further reason to select the resonance frequency

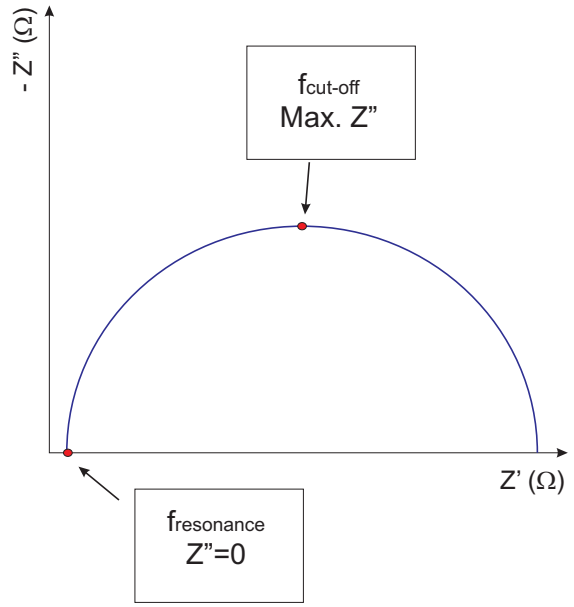


Fig. 4.21: Cut-off and resonance frequency

as base frequency: in this point the per-unit frequency is 1 p.u. Per-unit frequencies lower than one will automatically imply a capacitive behavior, while values higher will reflect an inductive behavior.

Albeit this resonance point is easily identifiable, it slightly decreases for increasing current, as depicted in Fig. 4.22. So, the previous base current(45 A) is the recommended decision criterion to select the base frequency. Considering that the steady-state base magnitudes were selected for rated values it is logical to infer that the base frequency should also be selected for rated current. Therefore, the base frequency chosen for the Nexa fuel cell is 2266.5 Hz (1 p.u.). Any frequency lower that the base frequency will be smaller to 1 p.u., instantly revealing the capacitive behavior, whilst frequencies larger than 1 p.u. will mean inductive behavior. These frequencies can be expressed as per-unit values with (4.15)

$$f\,(p.u.) = \frac{f\,(Hz)}{f_b\,(Hz)} \tag{4.15}$$

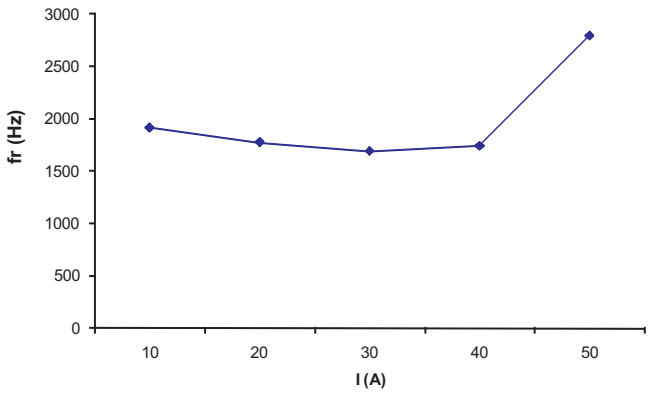


Fig. 4.22: Nexa fuel cell resonance frequency

## 4.5. Conclusions

Frequency domain tests, such as EIS, are a powerful tool to study the internal behavior of fuel cells. Moreover, it allows to model the fuel cell stack voltage operation through the fitting of an equivalent circuit. After fitting different types of equivalent circuits, the best approximation was found for the model presented. The inclusion of a diffusion element, such as the CPE allowed to fit more precisely the fuel cell impedance Nyquist plot. The suitability of a CPE versus an ideal capacitor has been demonstrated.

It has been observed that the developed temperature model takes into account the fuel cell fan due to the fact that the temperature time-constant decreases for increasing temperature. This is due to the fact that for increasing temperatures the fan sees its duty cycle increased, and causes a faster heat evacuation. However, as seen in the temperature model validation, the model is unable to exactly follow the temperature evolution during very high current loads, and affects the voltage model precision. This issue could be solved with a more detailed cooling model.

Finally, a per-unit system has been defined. Even though this was also presented by Choi, the per-unit system proposed in this work is a more general system, applicable to any type of load. This flexibility is due to the proposal of a base frequency, which can be defined when the current load presents a certain ac component superimposed to the dc operation point. Two different frequencies: cut-off and resonance frequency were studied as

possible base frequency. Finally, the resonance frequency was chosen due to its simple identification in Nyquist and Bode plots, as well as to the resistive impedance of the fuel cell at the resonance frequency. Any frequency lower to 1 p.u. will automatically imply a capacitive fuel cell behavior, whilst any frequency higher to 1 p.u. will include an inductive behavior.

CHAPTER 5

# *Nonlinear dynamic model for batteries*

## 5.1. Introduction

This chapter presents a nonlinear dynamic model of electrochemical batteries for simulation purposes, in both absolute and relative (per-unit) units, its deduction, development and validation. The battery studied is a sealed lead-acid battery, specially designed for traction purposes by Exide-Tudor [85]. Its principal characteristics are detailed in Table 5.1.

As explained previously a battery is an electrochemical system, which includes multiple aspects, such as thermal effects, fluid dynamics, electrochemical reactions, electrical phenomena, etc. Therefore, the model can be carried out from any of these points of view. However, the objective is to obtain a dynamic model which is able to yield information about its electric behavior, neglecting other effects which could be included. Moreover, it is desirable to obtain a model which can easily interact with other electric or electronic system models.

This electric model will adopt the form of an equivalent circuit which will be able to reproduce its current and voltage dynamic performance. The

| | | |
|---|---|---|
| Dimensions | Length | 260 mm |
| | Width | 173 mm |
| | Height | 207 mm |
| | Weight | 17,5 kg |
| Rated performance | Reserve capacity | 95 min |
| | C 5h | 45 Ah |
| | C 20h | 50 Ah |
| | SAE CCA (-18ºC) | 770 A |
| | EN CCA (-18ºC) | 800 A |
| | Cycles 2.5 % DOD | more than 200000 |
| | Cycles 17.5 % DOD | more than 3000 |
| | Vibration proof | EN 53342 V3 |
| Description | Connectors | 2 conical DIN terminals |
| | Colour | Grey |
| | Lid | Flat with centered gas outlet |
| Others | Charging procedure | 20 h/14,4 V+4 h/1,25 A |
| | Max. recc. voltage | 15 V |
| | Max. disch. load | 1000 A (30 s) |
| | Max. shorcirc. load | 1500 A (5 s) |

Table 5.1: Characteristics of the battery used

parameters of the resulting equivalent circuit will be obtained through electrochemical impedance spectroscopy EIS tests. Although the work is applied to a lead-acid battery, the experimental methodology and results can be extended to other technologies such as Ni-Mh, Li-ion, etc.

## 5.2. EIS tests experimental procedure

Electrochemical Impedance Spectroscopy EIS can be also applied to batteries, in a similar way as it was applied for fuel cells. However, the test procedure is slightly different due to the charge/discharge processes. Even if the main duty of a battery is to supply energy through discharge, depending on the final application, re-charging can also be a determinant process. Therefore, the final battery model should be able to reproduce both charge and discharge operation.

As in the case of the fuel cell, the battery current is more easily controlled

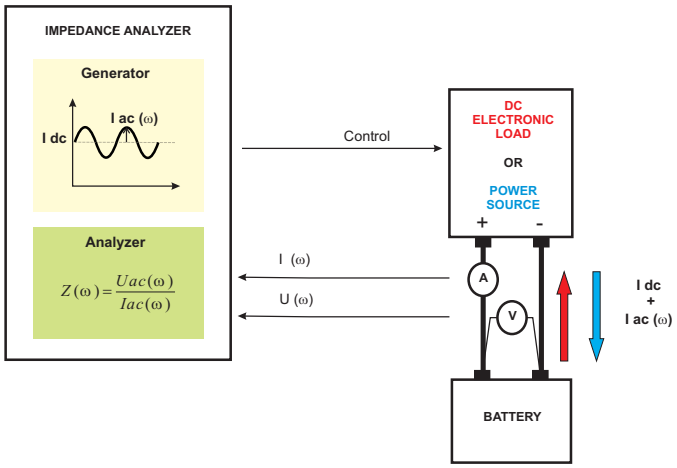


Fig. 5.1: *EIS* on batteries

than the voltage, galvanostatic (current control) mode tests are conducted, as, e.g. done by [64], [15] and [86]. Likewise, the battery is set to its dc operation current and a small signal ac current with variable frequency is superimposed. Both the dc+ac current components cause a dc+ac voltage response, which allows the obtention of the battery complex impedance taking into account only the ac components of the current and voltage signals, as depicted in Fig. 5.1.

### 5.2.1. DC operation conditions

A battery can operate in a wide range of states of charge (*SoCs*), either during charge or discharge processes within an also wide range of currents and temperatures. These facts play an important role in determining the number of tests necessary to characterize the battery.

A battery *SoC* can vary from fully discharged (0 %) to fully charged (100 %), however, it is not recommended to operate frequently at very low *SoCs* as it shortens the battery life. Therefore, the lower *SoC* at which tests are conducted has been set to 40 %. The selection criterion for the *SoC* upper limit is the battery voltage, which should not exceed the maximum voltage recommended by the manufacturer during charge (14.4 V for the battery under study). For high *SoCs* the battery can easily suffer overvoltage and overcharge; hence, the maximum *SoC* considered is 90 %.

The battery used can either supply or absorb very high currents (up to 1000 A discharge during 30 s). To select the dc operation values at which the EIS tests are carried out, two facts have to be taken into account. The first one is related to the lower current limit. If the lower limit is too small, the results obtained from the model will be incorrect due to the considerable noise component in the current and voltage signals. Therefore, 2.5 A is selected as the minimum dc current. The second fact which must be taken into account is that the test conditions (current, voltage, $SoC$) should be kept within a narrow interval. For example, if tests are carried out at very high currents, the battery $SoC$ will vary more than 10 % from the beginning to the end of the test, invalidating the results obtained. This will limit the maximum current to 20 A.

The maximum and minimum current operation, the test duration and the room temperature will influence the battery operation temperature. If the battery current is kept low, the test duration is less than 15 minutes, then the battery temperature can be considered to be constant and equal to the room temperature (25°C). Therefore, tests will be carried out for the following operation conditions:

- Process: charge and discharge.
- DC current: 2.5, 5, 10 and 20A.
- $SoC$: 40, 50, 60, 70, 80 and 90 %.

### 5.2.2. AC test conditions

As pointed out previously, a current ac signal is superposed to the dc current, allowing to carry out the EIS test during the normal battery operation. However, the ac signal should not disturb substantially the operation conditions (current, voltage, $SoC$ and temperature). Therefore, in all EIS tests the ac selected signal presents a low amplitude which is dependant on the dc operation current. The ac current ripple should be much smaller than the dc current level; therefore, the ac signal amplitude is defined as a certain percentage of the dc operation current. Different ac-dc current relationships can be investigated, as presented in Chapter 3, but for this work the ac signal

amplitude selected is a 5 % of the dc current, as higher values would provoke ac voltages greater than 0.25 % of the rated voltage (12 V) and lower values would present a high noise component [54].

The frequency of the ac ripple is variable and sweeps from its minimum frequency to its maximum frequency. Due to the fact that each of the phenomenon which takes place in a battery is revealed at different frequencies, it is necessary to subject the battery to a frequency sweep. This sweep can vary from low frequencies ($\mu$Hz) to high frequencies (kHz-MHz), as explained in [87]. However, it is not possible to carry out such a wide interval of frequencies due to the duration of the tests. For example, if very low frequencies were explored, the test time could lengthen for hours, which would provoke a variation of the test conditions, especially in temperature and *SoC*. Therefore, the minimum frequency is set at 0.1 Hz, whilst the maximum frequency is selected at 6 kHz. The upper frequency is selected at 6 kHz as higher frequencies would not reveal more relevant information and above 6kHz the measures include more noise. This is especially true in the case of the electronic load and the power source, which can present difficulties in following high frequency signals.

### 5.2.3. Experimental setup

To carry out the EIS tests the following equipment has been used:

- Impedance analyzer (Solartron 1260).
- DC electronic load (Chroma 63201: 80 V, 300 A).
- DC power source (Sorensen 20-150E: 20 V, 150 A).
- LEM LA 305-S current transducer.
- $\pm$15 V power source for transducer supply.
- Computer.
- Exide-Tudor 12 V lead-acid battery.

For both the discharge and charge processes, the impedance analyzer controls the whole test through the software Zplot by programming the dc

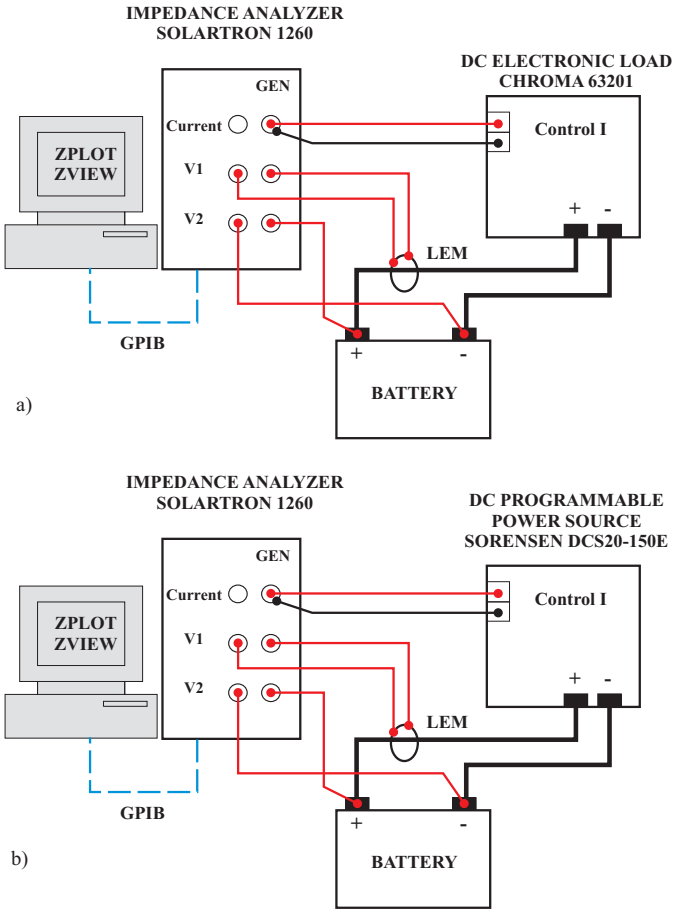


Fig. 5.2: Experimental setup for battery EIS tests for a) discharge b) charge

electronic load (during discharge processes) or the dc power source (during charge processes) externally with a 0-10 V signal, imposing the dc and ac current the battery should sink or supply. The battery current is measured by the LEM transducer and sent to the impedance analyzer, whereas the voltage is directly measured by the impedance analyzer at the battery terminals to avoid the influence of the power cables on the impedance calculation. Fig. 5.2 depicts the power and control connections between the different equipments involved for both charge and discharge tests and Fig. 5.3 shows a photograph of the setup.

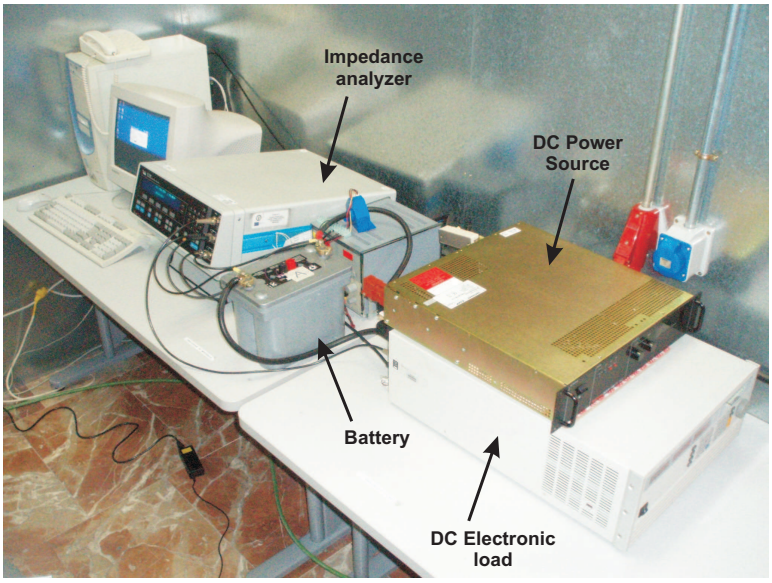


Fig. 5.3: EIS tests experimental setup photograph

## 5.3. EIS tests results: battery impedance model

EIS tests were conducted for both charge and discharge processes, as it can be found in [16], so two different equivalent circuits are obtained for the battery. Once all the tests are completed, the measurements obtained are processed with the software ZView, licensed by the impedance analyzer manufacturer. This software allows plotting the Nyquist and Bode plots for the battery impedance and adjust it to an equivalent circuit, whose topology is proposed by the user. Figs. 5.4 and 5.5 presents the results for one of the cases, at 70 % SoC at 2.5, 5 and 10 A. Z" represents the imaginary part of the complex impedance while Z′ represents the real part. If Fig. 5.4 is read from the upper to the lower part, it can be observed that the battery shows a capacitive behavior (negative imaginary part) at low frequencies, whilst it behaves as an inductive impedance (positive imaginary part) at higher frequencies.

The capacitive behavior is reflected by a curve which resembles two circumferences, one with a smaller diameter than the other, as reflected in Fig. 5.6, and also reported by [16], [64], [88], [67]. The maximum of each circumference corresponds to the so called cut-off frequency, which corresponds to

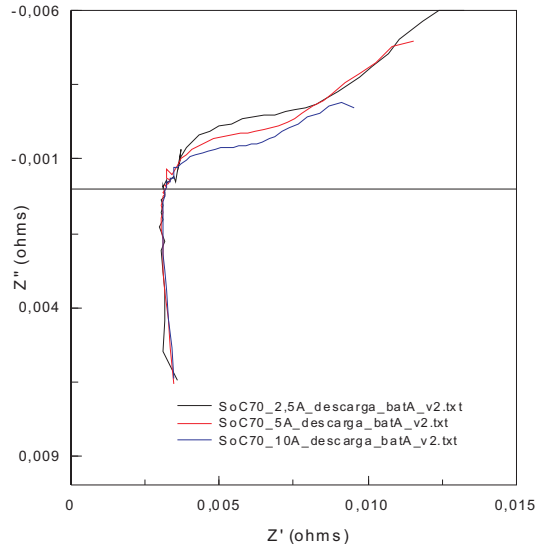


Fig. 5.4: Nyquist diagram for 70 % $SoC$ during discharge

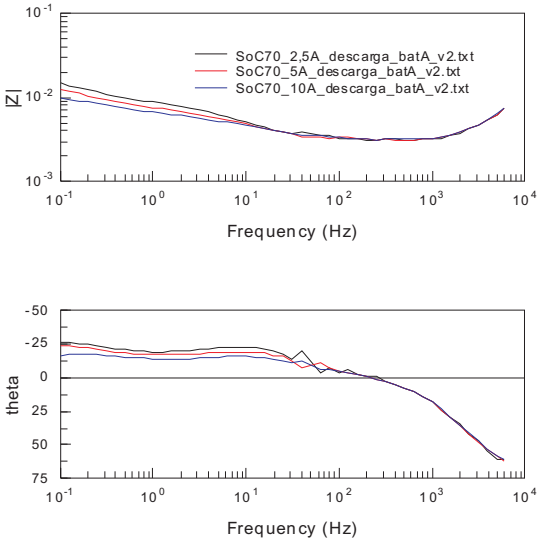


Fig. 5.5: Bode diagram for 70 % $SoC$ during discharge

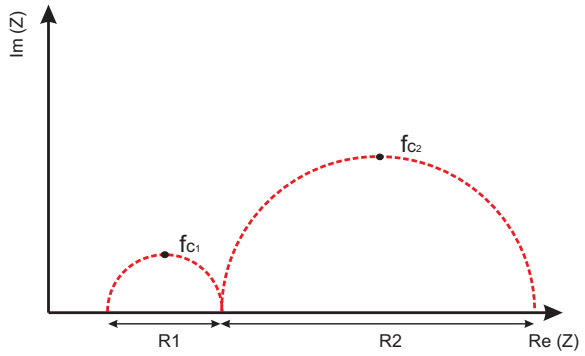


Fig. 5.6: Approximation of the Nyquist plot

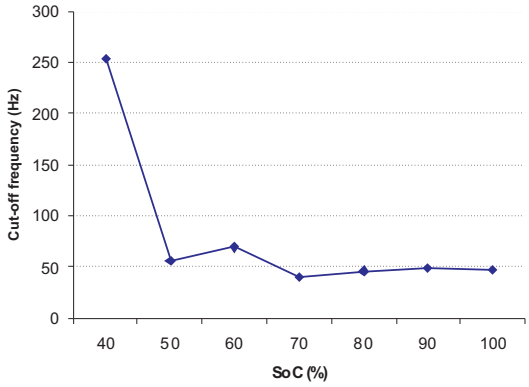


Fig. 5.7: Cut-off frequency evolution with $SoC$

the point where the imaginary part of the RC network impedance reaches its maximum value. The cut-off frequency is not constant, but shows a well defined trend, as a function of the $SoC$ for the anode electrode which is shown in Fig 5.7. The frequency is high for low $SoCs$, and is around 50 Hz for the rest of $SoCs$.

As seen in Chapter 3, a circumference in a Nyquist plot corresponds to a RC network. In this case, there are two different circumferences and each of them corresponds to a different RC network.

The bigger circumference can be encountered at low frequencies, which can range from 100 $\mu$Hz to 1 Hz (from 0.1 Hz in this work). At these frequencies the dominant phenomenon is the diffusion inside the porous electrodes [89]. As reported by [87], diffusion can be located either in the electrolyte or the electrodes. Diffusion is created in the electrolyte due to the move-

ment of ions, which must travel from the electrode were they are produced to the other electrode, in which they are consumed. However, the most relevant diffusion takes part in the electrodes. As electrodes are porous, the electrochemical reaction can take place both inside or on the surface of the electrode, and is precisely this fact summed up with the presence of pores which provoke the diffusion. More information about these phenomena can be consulted in [39], [69].

The smaller circumference which represents an RC network describes the behavior at intermediate frequencies (from 1 Hz to 1 kHz) and represents the charge transfer reaction and the double layer capacitance, which occur in parallel due to the fact that both the double-layer capacitor and the electrochemical charge transfer appear on the electrode surface [89].

The double layer capacitor is similar to the one described for the fuel cell and can be represented as a capacitance in parallel to the charge transfer resistance.

The inductive behavior of the battery appears at high frequencies ($>$ 1 kHz) and is represented in the Nyquist plot by a line, which is not totally vertical, but slightly curved to the right. This small curvature is due to the skin effect present at very high frequencies. At these frequencies, the penetration depth of the current in the conductors lessens, increasing the real part of the complex impedance. This penetration depth depends on the material proprieties, particulary on the inverse of the conductivity square root and the inverse of the frequency square root [87].

When the imaginary part of the impedance is zero, the impedance becomes purely resistive. This point represents the smallest impedance value for the whole curve. The corresponding frequency (resonance frequency) is not constant, but dependant on the battery $SoC$, and is depicted in Fig. 5.8 from the EIS test carried out. As it happened for the cut-off frequency, the value for low $SoCs$ is higher than for the rest of $SoCs$. This trend has also been observed by [72]. For the battery studied in this Thesis, the resonance frequency is comprised between 265 Hz and 190 Hz.

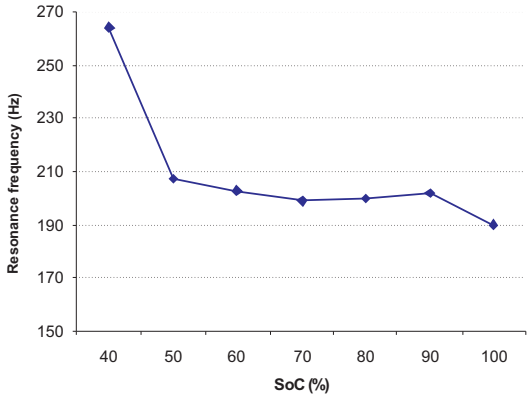


Fig. 5.8: Resonance frequency evolution with $SoC$

With the Nyquist plots for the all the $SoCs$ at the different currents, an equivalent circuit, as the one shown in Fig. 5.9 can be obtained for each of the EIS tests.

Once all the EIS tests data has been process with ZView, as shown in Fig. 5.9, it is possible to study the effect of current and $SoC$ on the battery impedance. To do so, the statistical software, Statgraphics, is used. A multivariable analysis has been carried out for each parameter of the equivalent circuit. For example, the statistical analysis carried out for $R_2$ is displayed in Fig. 5.10.

One of the plots returned by Statgraphics is the Observed vs. Predicted chart, in which the best possible plot is when all the points are on the $45^{o}$ line, which would mean that the model parameters are identical to the observed values.

With the previous results a passive dynamic nonlinear model for the battery which distinguishes a charge from a discharge process is obtained and depicted in Fig. 5.11. The parameters equations during discharge are given in (5.1).


| Element | Freedom | Value | Error | Error % |
|---|---|---|---|---|
| L | Free(+) | 1,8589E-7 | 3,7982E-9 | 2,0433 |
| Rohm | Free(+) | 0,0034064 | 3,2615E-5 | 0,95746 |
| R1 | Free(+) | 0,010322 | 0,00068629 | 6,6488 |
| C1 | Free(+) | 171,8 | 6,7805 | 3,9467 |
| R2 | Free(+) | 0,0026366 | 7,3451E-5 | 2,7858 |
| C2 | Free(+) | 4,421 | 0,2483 | 5,6164 |

| | |
|---|---|
| Chi-Squared: | 0,0088829 |
| Weighted Sum of Squares: | 0,81723 |
| Data File: | D:\TESIS\ENSAYOS\ENSAYO EIS BATERIA\CON SE |
| Circuit Model File: | D:\TESIS\ENSAYOS\ENSAYO EIS BATERIA\CON SE |
| Mode: | Run Fitting / Freq. Range (0,1 - 6000) |
| Maximum Iterations: | 100 |
| Optimization Iterations: | 0 |
| Type of Fitting: | Complex |
| Type of Weighting: | Calc-Modulus |

Fig. 5.9: Equivalent circuit obtained through ZView

$$
\begin{aligned}
L(H) &= 1{,}72 \cdot 10^{-7} - 2{,}25 \cdot 10^{-11} \cdot SoC \\
R_{ohm}(\Omega) &= 4{,}25 \cdot 10^{-3} - 6{,}13 \cdot 10^{-7} \cdot SoC^2 + 5{,}68 \cdot 10^{-7} \cdot SoC^3 \\
R_1(\Omega) &= 0{,}013 - 1{,}51 \cdot 10^{-3} \cdot I + 6{,}06 \cdot 10^{-5} \cdot I^2 + 2{,}24 \cdot 10^{-7} \cdot SoC^2 \\
C_1(F) &= 174{,}131 - 0{,}42 \cdot I^2 - 0{,}21 \cdot SoC^2 + 4{,}73 \cdot 10^{-3} \cdot SoC^3 - 2{,}68 \cdot 10^{-5} \cdot SoC^4 \\
R_2(\Omega) &= 9{,}30 \cdot 10^{-4} - 7{,}15 \cdot 10^{-5} \cdot I^2 + 5{,}45 \cdot 10^{-6} \cdot I^3 + 1{,}61 \cdot 10^{-6} \cdot SoC^2 - \ldots \\
&\quad \ldots - 1{,}22 \cdot 10^{-8} \cdot SoC^3 \\
C_2(F) &= 5{,}74 + 0{,}01 \cdot I^2
\end{aligned}
\tag{5.1}
$$

## 5.4. Tests for the determination of the battery internal voltage

The battery equivalent circuit shown in Fig. 5.11 is a passive circuit, which needs a power source or similar element to represent the active nature of the battery. This active element is a voltage source which represents the open circuit voltage $OCV$, which is dependant on the $SoC$, as recorded in the literature by [90], [16] and [91].

```
Multiple Regression Analysis
-------------------------------------------------------------------------------
Dependent variable: R2
-------------------------------------------------------------------------------
                                        Standard          T
Parameter               Estimate          Error       Statistic        P-Value
-------------------------------------------------------------------------------
CONSTANT                0,0101726     0,00420623        2,41845         0,0420
I^2                  0,0000319902  0,00000559691        5,71569         0,0004
SOC                  -0,000431785    0,000151369       -2,85254         0,0214
SOC^2                0,00000545876  0,00000130864        4,17132         0,0031
-------------------------------------------------------------------------------

                          Analysis of Variance
-------------------------------------------------------------------------------
Source              Sum of Squares     Df  Mean Square    F-Ratio       P-Value
-------------------------------------------------------------------------------
Model                 0,0000755932      3 0,0000251977      52,95         0,0000
Residual              0,00000380678     8   4,75848E-7
-------------------------------------------------------------------------------
Total (Corr.)         0,0000793999     11

R-squared = 95,2056 percent
R-squared (adjusted for d.f.) = 93,4076 percent
Standard Error of Est. = 0,000689817
Mean absolute error = 0,00045577
Durbin-Watson statistic = 1,19645


The StatAdvisor
---------------
   The output shows the results of fitting a multiple linear
regression model to describe the relationship between R2 and 3
independent variables.  The equation of the fitted model is

R2 = 0,0101726 + 0,0000319902*I^2 - 0,000431785*SOC +
0,00000545876*SOC^2

Since the P-value in the ANOVA table is less than 0.01, there is a
statistically significant relationship between the variables at the
99% confidence level.
```

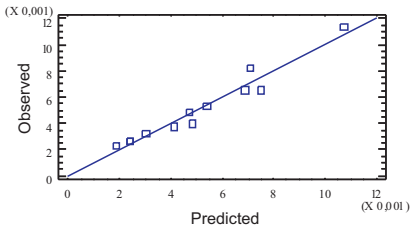


Fig. 5.10: Statistical analysis for $R_2$

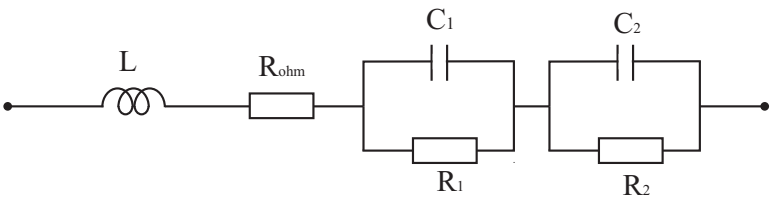


Fig. 5.11: Equivalent circuit for the battery impedance

This relationship between the $OCV$ and the $SoC$ differs also during charge/discharge process. When the whole charge/discharge cycle is considered, this causes a sort of hysteresis effect on the $OCV$ curve due to the battery surface charge. In fact,when the battery is charged, the charge accumulates on the electrode surface and then diffuses through the electrodes [16], [91]. This diffusion process is slower than the ions transport across the electrolyte, provoking a charge accumulation on the electrode surface, and hence an increase of the battery voltage. This phenomenon is rarely taken into account by other authors, even if it does affect the final accuracy of the model.

To calculate the $OCV$ for the battery under study after a charge or discharge process, the battery is charged to a 100 % $SoC$ following the standard UNE-EN 50342-1 [92], which details that the battery should be charged with a constant voltage of 14.4 V during 20 h, with a $5{\cdot}I_{rated}$ current limitation, followed by a constant current charge of $0.5{\cdot}I_{rated}$ during 4 h.

To obtain the $OCV$ curve after a discharge process, successive pulse discharges of 10 A with 15 min rest between pulses were applied to the battery until the 30 % of $SoC$ was reached, as detailed in Table 5.2.

From the $SoC$ reached at the end of the previous tests, successive charging current pulses are applied with 45 minutes rest between pulses. In this case the rest time is longer than after a discharge due to the slower diffusions processes. During this process, the charge current is reduced for increasing $SoC$ to avoid overvoltage, which could endanger the battery. Another difference with the discharge procedure is that for a charge process the charge efficiency should be taken into account. This efficiency reflects that not all the energy injected to the battery is used for its charging due to the effect of irreversible processes such as gasification during overcharging [93]. The charge efficiency is smaller for high $SoCs$, when the battery presents a higher opposition to accept charge, needing small values of currents during large periods of time to complete the charging process. The experimental procedure for the $OCV$ obtention after a charge process is detailed in Table 5.3.

The hysteresis curve for the $OCV$ obtained is depicted in Fig. 5.13. The

| SoCinitial (%) | ΔSoC (%) | SoCfinal (%) | Discharge time* (h) |
|---|---|---|---|
| 100 | 5 | 95 | 0.25 |
| 15 min rest | | | |
| 95 | 5 | 90 | 0.25 |
| 15 min rest | | | |
| 90 | 10 | 80 | 0.5 |
| 15 min rest | | | |
| 80 | 10 | 70 | 0.5 |
| 15 min rest | | | |
| 70 | 10 | 60 | 0.5 |
| 15 min rest | | | |
| 60 | 10 | 50 | 0.5 |
| 15 min rest | | | |
| 50 | 10 | 40 | 0.5 |
| 15 min rest | | | |
| 40 | 5 | 35 | 0.25 |
| 15 min rest | | | |
| 30 | 5 | 30 | 0.25 |

*Discharge time: $t\,(h) = \frac{\Delta SoC(\%) \cdot C_n}{I(A) \cdot 100}$

Table 5.2: Experimental procedure to calculate the $OCV$ after discharge

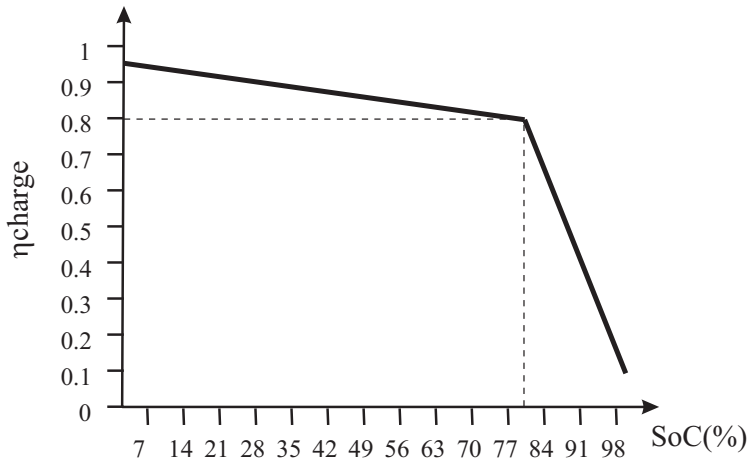


Fig. 5.12: Charge efficiency

| SoCinitial (%) | ΔSoC (%) | SoCfinal (%) | I (A) | $\eta$ | Charge time* (h) |
|---|---|---|---|---|---|
| 30 | 5 | 35 | 20 | 0.89 | 0.14 |
| 45 min rest | | | | | |
| 35 | 5 | 40 | 20 | 0.884 | 0.14 |
| 45 min rest | | | | | |
| 40 | 10 | 50 | 20 | 0.875 | 0.285 |
| 45 min rest | | | | | |
| 50 | 10 | 60 | 10 | 0.856 | 0.584 |
| 45 min rest | | | | | |
| 60 | 10 | 70 | 5 | 0.83 | 1.2 |
| 45 min rest | | | | | |
| 70 | 10 | 80 | 5 | 0.818 | 1.22 |
| 45 min rest | | | | | |
| 80 | 10 | 90 | 1 | 0.8 | 6.25 |
| 45 min rest | | | | | |
| 90 | 5 | 95 | 0.5 | 0.45 | 11.11 |
| 45 min rest | | | | | |
| 95 | 5 | 100 | 0.5 | 0.275 | 18.18 |

*Discharge time: $t\,(h) = \frac{\Delta SoC(\%) \cdot C_n}{\eta \cdot I(A) \cdot 100}$

Table 5.3: Experimental procedure to calculate the $OCV$ after charge

equations obtained with Statgraphics for the charge and discharge cycle are presented in (5.2), whilst the observed versus predicted curves for each equations are shown in Fig. 5.14. The determination of the $OCV$ completes the development of the active model.

$$\begin{aligned} OCV_{dis.} &= 11{,}5648 - 0{,}00759 \cdot SoC + 0{,}00148 \cdot SoC^2 - ... \\ &\quad ... - 3{,}5 \cdot 10^{-5} \cdot SoC^3 + 3{,}61 \cdot 10^{-7} \cdot SoC^4 - 1{,}34 \cdot 10^{-9} \cdot SoC^5 \\ OCV_{char.} &= 13{,}9733 - 0{,}3276 \cdot SoC + 0{,}01769 \cdot SoC^2 - ... \\ &\quad ... - 4{,}1 \cdot 10^{-4} \cdot SoC^3 + 4{,}4 \cdot 10^{-6} \cdot SoC^4 - 1{,}79 \cdot 10^{-8} \cdot SoC^5 \end{aligned} \tag{5.2}$$

## 5.5. Complete battery model

The final structure of the active nonlinear dynamic model of the battery is represented in Fig. 5.15. The voltage at the battery terminals is calculated

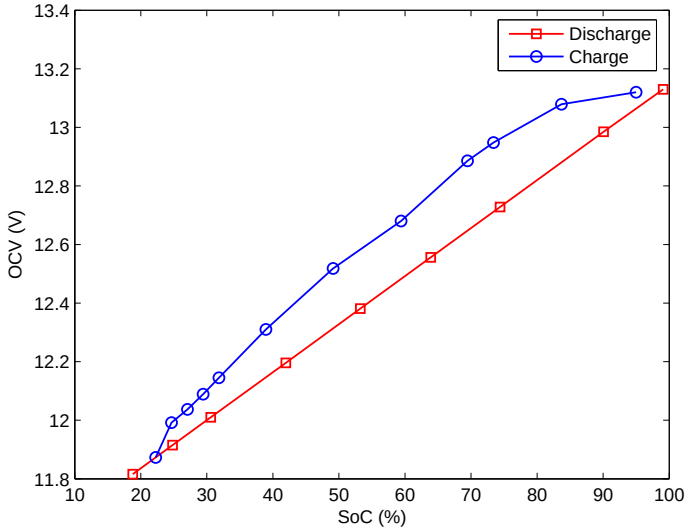


Fig. 5.13: Hysteresis curve for $OCV$

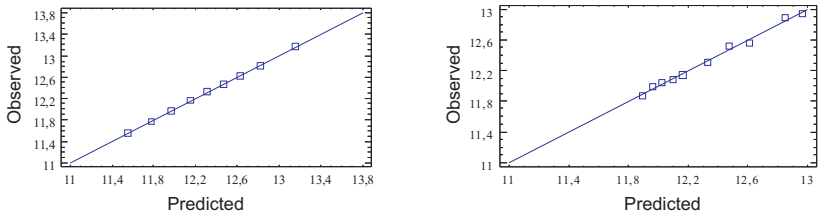


Fig. 5.14: Statgraphics observed vs. predicted curves for $OCV$ during discharge (left) and charge (right)

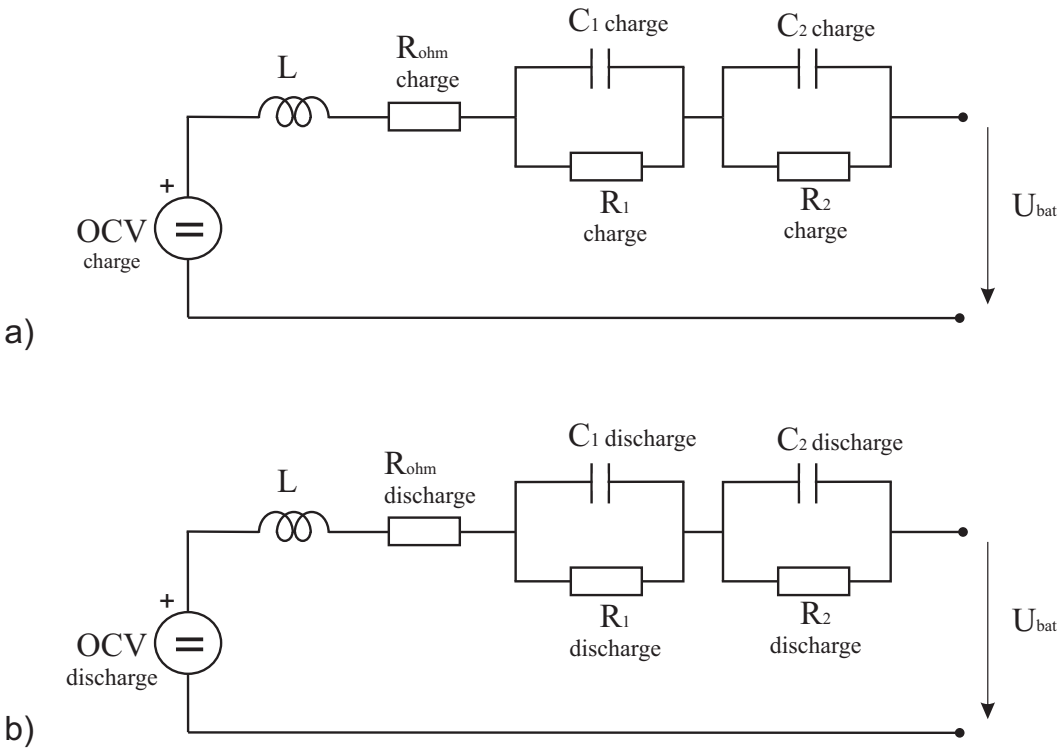


Fig. 5.15: Active equivalent circuit of the battery for a)charge and b)discharge

in (5.3).

$$\begin{aligned} U_{bat} &= OCV - U_L - U_{R_{ohm}} - U_{C_1} - U_{C_2} \\ U_L &= L \cdot \frac{dI}{dt} \\ U_{R_{ohm}} &= R_{ohm} \cdot I \\ U_{C_1} &= \int \frac{1}{C_1} \cdot \left( I - \frac{U_{C_1}}{R_1} \right) \cdot dt \\ U_{C_2} &= \int \frac{1}{C_2} \cdot \left( I - \frac{U_{C_2}}{R_2} \right) \cdot dt \end{aligned} \tag{5.3}$$

### 5.5.1. State of charge calculation

To reproduce the behavior of a battery, not only the voltage dynamic should be emulated, but also the battery state of charge $SoC$, which is a percentage of the rated capacity and indicates the battery useful capacity.

The battery $SoC$ calculation is not a trivial issue [94], [69], especially for non-flooded batteries, as, the acid concentration of the electrolyte, which is

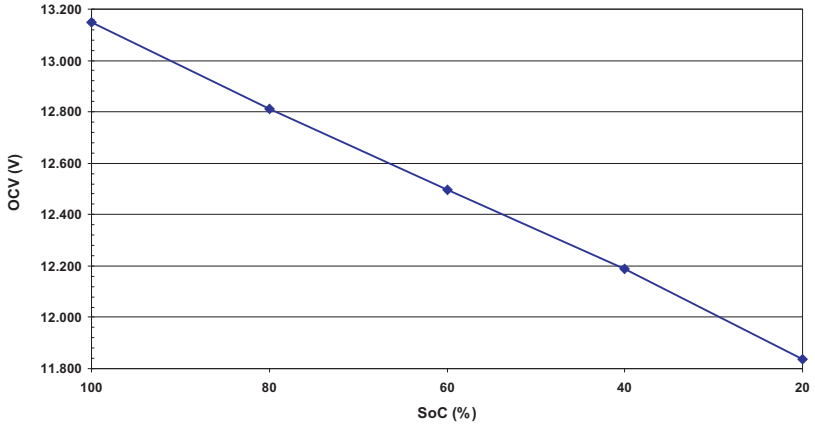


Fig. 5.16: $OCV$ vs. $SoC$

a good indicator of the battery $SoC$, cannot be directly measured. Hence, the $SoC$ needs to be estimated indirectly, through the measurement of other variables such as current and time or voltage.

In this Thesis two methods for the calculation of the $SoC$ have been applied. In the first method the $SoC$ is linearly dependant on the open circuit voltage $OCV$, as depicted in Fig. 5.16, which was an information supplied by Exide-Tudor. The advantage of this method is its simplicity, however, it presents a serious drawback, related to the time the battery should rest before the $OCV$ can be measured. This rest time is needed to allow diffusion phenomena to take place in order to allow the voltage to reach its steady state point. Depending on the process which the battery has suffered previous to the $OCV$ measurement, the rest time can vary from 30 minutes if a discharge has taken place before, to hours if it was a charging process. This rest time can be critical for certain applications, such as electric or hybrid vehicles, in which the driver cannot wait hours to know the battery $SoC$. Therefore, this method can only be applied before the use of the battery, to calculate the initial $SoC$, or after a full recharge.

The second method used to measure the $SoC$ consists in the integration of the battery current with respect to time. This method can be applied under operating conditions, provided the initial $SoC$ is known due to the

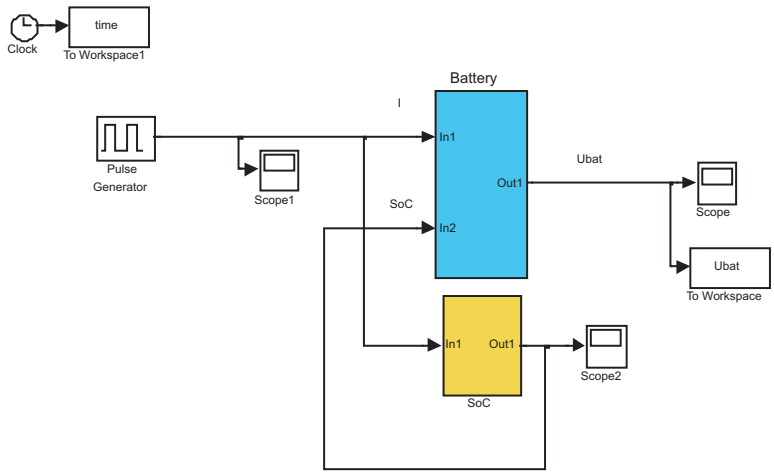


Fig. 5.17: Matlab/Simulink model for the battery

$OCV$ measurement.

$$SoC_t(\,\%) = SoC_{t-1} \pm \frac{\eta}{C_n} \cdot \int_{t-1}^{t} I(t)dt \cdot 100 \tag{5.4}$$

The equation takes into account the previous $SoC$ and the charge efficiency $\eta$.

The model obtained for the battery is implemented in Matlab/Simulink, taking into account the different parameters of the equivalent circuit, that may be different if the process is either a charge or discharge one. Figs. 5.17 and 5.18 represent the block model in Matlab/Simulink. The current profile in Fig. 5.19 has been applied to the real battery and model, and the experimental and modeled voltage profile obtained is depicted in Fig. 5.20.

If instead of a discharge cycle the battery undergoes a charge cycle, the charge current profile is depicted in Fig. 5.21 and the corresponding experimental and modeled voltage in Fig. 5.22.

## 5.6. Per-unit approach to batteries

All the battery models developed heretofore, including the one described above represent the electrical behavior of batteries by means of an equivalent circuit whose variables include voltages (V), currents (A), impedances ($\Omega$)

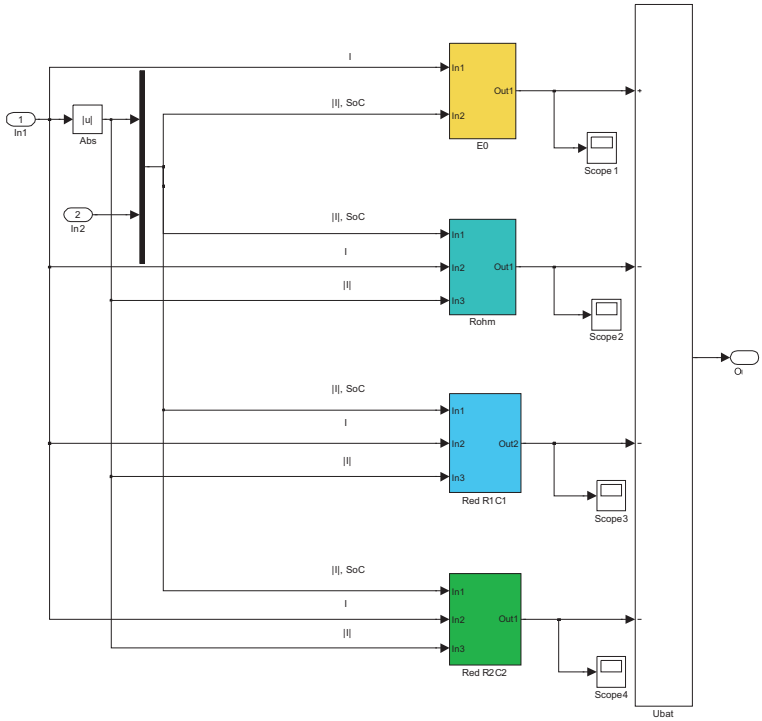


Fig. 5.18: Detail of the Matlab/Simulink model

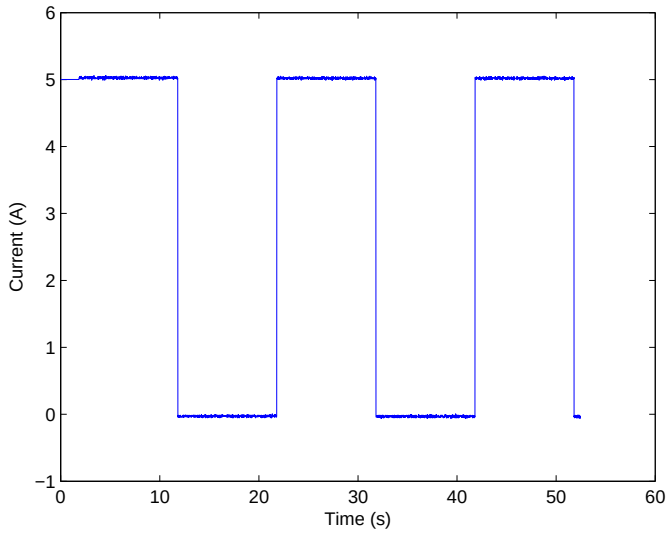


Fig. 5.19: Discharge current profile required to the battery

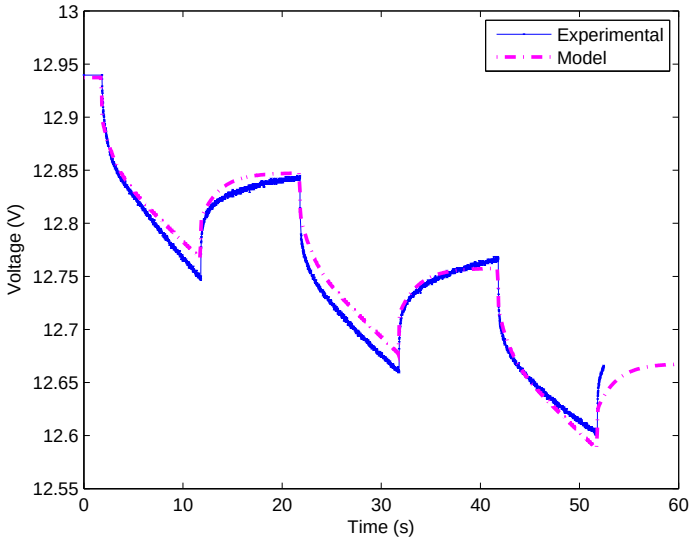


Fig. 5.20: Experimental and modeled battery voltage during discharge

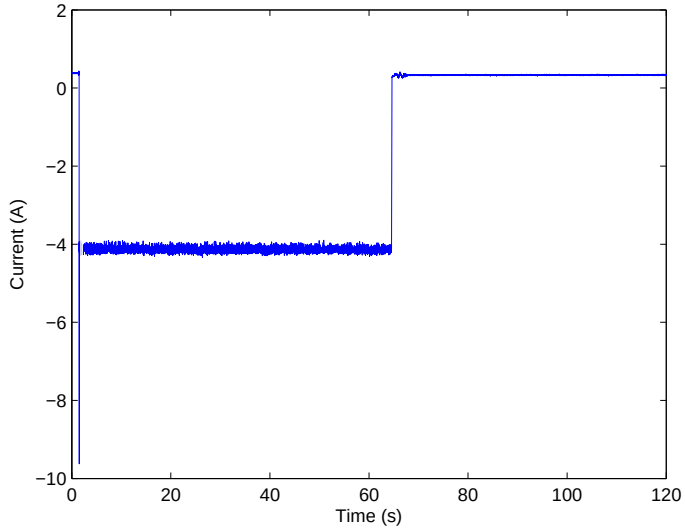


Fig. 5.21: Charge current profile injected in the battery

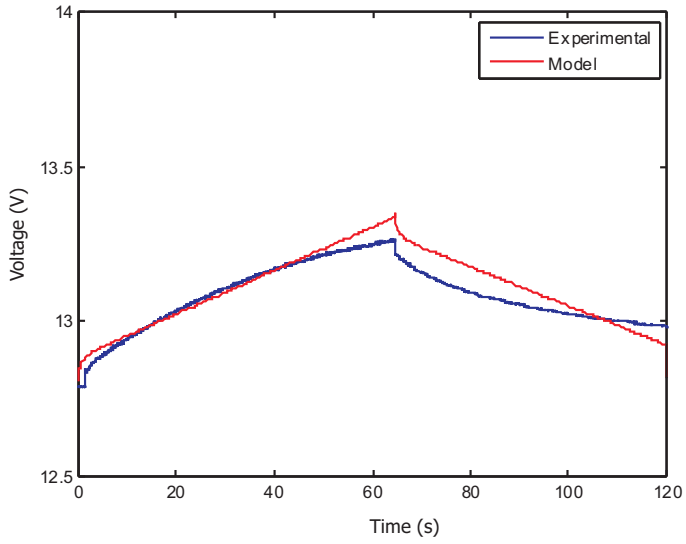


Fig. 5.22: Experimental and modeled battery voltage during charge

and power (W), i.e. in absolute magnitudes. This approach corresponds to the basic way power engineers solve electrical circuits and power systems.

But this classic approach needs to be changed when energy storage systems, such as batteries are incorporated to a power system. With this classic point of view, the general assumption is that the energy delivered by the power sources is unlimited. This may be true for other power sources, but not for batteries or other energy storage system. Apart from voltage, current, power and impedance storage systems are not completely defined without an additional variable: the available energy stored and ready to be delivered at a given instant.

For the analysis of power systems which present different voltage levels, the usual way to describe the variables is in per-unit values (p.u.) relative to a defined set of base values. The usual set of variables are power, voltage, current and impedance. However, when energy comes into play a new base magnitude needs to be included: the base time. Time is taken into account in the variable "battery capacity", expressed in Amperes hour (A·h), which is the product of the rated current times the rated discharge time. Therefore, the classic base magnitudes have to be revised and new magnitudes included.

| Author | Voltage (V) | Capacity (A·h) | *Rohm* (mΩ) |
|---|---|---|---|
| Blanke [72] | 12 | 70 | 5.2 |
| Gauchia | 12 | 50 | 3.2 |
| Hariprakash [71] | 6 | 4 | 75 |
| Karden [88] | 4 | 100 | 0.6 |
| Salkind [15] | 12 | 100 | 6.5 |
| Salkind [15] | 6 | 10 | 5 |

Table 5.4: Comparison between different authors

Curiously, there is a mixture of per-unit and absolute variables which have been used by both electrochemical and power engineers. For example, voltage is expressed in V, current in A, but battery state of charge is defined as a percentage, that is, a dimensionless variable. In most cases, for electrochemical systems, power engineers inherit the vocabulary established by electrochemical engineers, even if an obvious different focus is given, but no in depth transformation has been done to adapt the inherited variables to the power engineering world. Furthermore, the current situation collides with the usual way power engineers use to represent and analyze the electrical power system.

The drawbacks of this mixed per-unit and absolute variables are clearly exposed when a comparison between the performance of batteries with different characteristics, or a sizing calculation is carried out. The variables, such as voltage, capacity, impedance, power, etc. can assume a wide range of values as they are dependant on the overall size of the system, defined by its rated capacity, voltage or current. For example, if one of the parameters of the equivalent circuit calculated previously is compared to those obtained by other authors, no clear conclusion about the correctness of the results can be concluded. Table 5.4 presents the results for the ohmic resistance at 70 % obtained by several authors.

Analyzing Table 5.4, no clear relationship can be extracted, as batteries with similar voltages and capacities exhibit very different impedances. Therefore, how can any author compare its results to those obtained by other authors?

This Thesis proposes the application of a per-unit system to batteries to

overcome these problems, explaining the need to use two different base times, in order to represent phenomena which occur in different time horizons, as it is the case of the long-term charge/discharge processes versus the transient phenomena. To this end, an equivalent circuit for a battery will be developed and its parameters will be calculated and represented as per-unit values. Finally, the proposed methodology will be applied to different cases referred in the bibliography and compared with experimental results obtained for this work.

### 5.6.1. Steady-state per-unit system for a battery

For energy storage devices such as batteries, the usual base variables used (voltage, current, power and impedance) is inadequate, as a base value for the energy stored or released by the battery must be defined. Hence, it is essential to introduce the concept of capacity, which is related with the discharge duration according to the Peukert equation [62].

$$C \cdot I^{pc-1} = constant \tag{5.5}$$

Where $C$ is the rated capacity, $I$ the current and $pc$ the Peukert coefficient (usually between 0.5 and 2), which is unique for each technology and model. The equation reveals that the available capacity at constant discharge current is reduced for increasing discharge rates.

Therefore, a new set of base magnitude which includes a base capacity $C_b$ related to a discharge time $t_b$ must be created. Known the base capacity and the discharge time (information which can be easily found in the data sheet handed by the manufacturer), the base current can be obtained.

$$I_b\,(A) = \frac{C_b}{t_b} \tag{5.6}$$

If the "natural" choice of taking the open circuit voltage as base voltage is adopted, the rest of base values can be obtained, completing the set of base values necessary to describe the battery performance for stationary operation. All the base values are presented in Table 5.5. Evidently, if three values are suitably selected, the rest of the base values can be calculated. However, the selection criterion of the first three base values is not arbitrary as the base

| Base capacity | Base discharge time | Base current | Base voltage | Base power | Base impedance |
|---|---|---|---|---|---|
| $C_b$ (A· h) | $t_b$ (h) | $I_b$ (A) | $U_b$ (V) | $P_b$ (W) | $Z_b$ (Ω) |

Table 5.5: Proposed base variables for a battery

| Author | U (V) | C (Ah) | t (h) | R (mΩ) | Ib (A) | Zb (Ω) | R (p.u.) |
|---|---|---|---|---|---|---|---|
| Blanke | 12 | 44 | 20 | 5,2 | 2,2 | 5,45 | 0,95 |
| Gauchia | 12 | 50 | 20 | 3,2 | 2,5 | 4,8 | 0,67 |
| Hariprakash | 6 | 4 | 5 | 75 | 0,8 | 7,5 | 10 |
| Karden | 4 | 100 | 10 | 0,6 | 10 | 0,4 | 0,24 |
| Salkind | 12 | 100 | 20 | 6,5 | 5 | 2,4 | 2,7 |
| Salkind | 6 | 10 | 20 | 5 | 0,5 | 12 | 0,42 |

Table 5.6: Proposed base variables for a battery

values must be linearly independent.

$$P_b = U_b \cdot I_b \qquad Z_B = \frac{U_b}{I_b} \tag{5.7}$$

Table 5.6 completes Table 5.4 by adding the base magnitudes and by expressing the resistances in p.u. values. The base current is calculated known the discharge time for which the capacity is defined. The base impedance can be calculated as the ratio of the base voltage (rated value) and base current.

The comparison between the resistance values in absolute and per-unit values yields different information about the relationship between them. For example, the resistance obtained by Karden is one order of magnitude smaller than the one presented by Blanke or the obtained in this Thesis. No linear relationship can be found with voltage or capacity, which was also pointed out by Karden [88]. However, the three mentioned values are near enough when compared as p.u. values. Therefore, the comparison between absolute values can be misleading, as the capacity of the batteries influences, for example, the impedance.

### 5.6.2. Per unit representation of the discharge curve

The discharge curve is an extended representation of the evolution of the battery voltage with the discharged capacity. Its frequent use makes it ad-

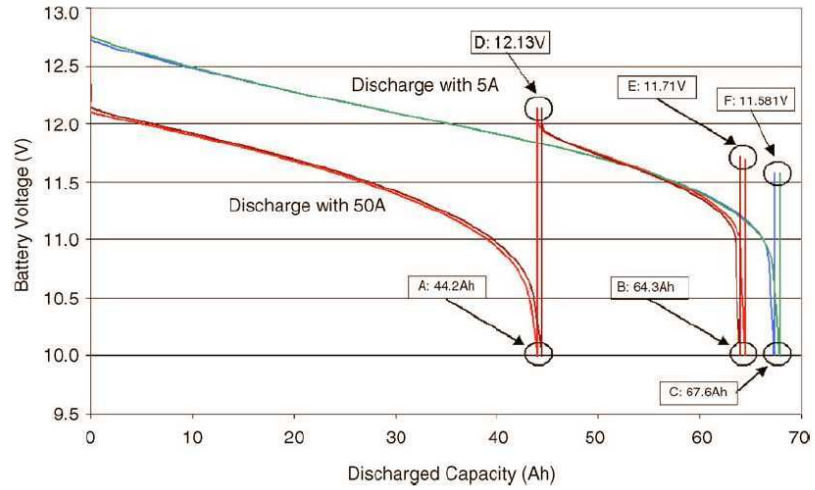


a)

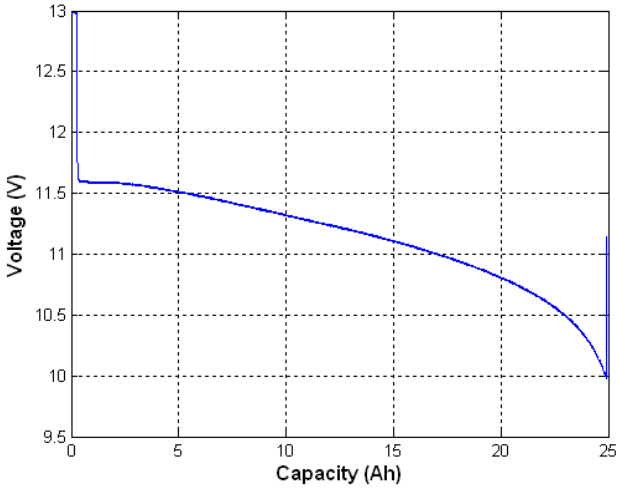


b)

Fig. 5.23: Discharge curve obtained by a)Doerffel and b)Gauchia in absolute values

visable to define it in per-unit values, in order to allow a direct comparison between curves obtained for different batteries, which can proceed from different manufacturers or can be from different technologies.

Fig. 5.23 a, taken from Doerffel [63] represents experimental results in which a battery apparently discharged at high discharge rate can be further discharged at a lower discharge rate, all variables being expressed in absolute values in the original work. Fig. 5.23 b represents a discharge curve obtained for the Exide-Tudor battery used in this Thesis.

| Base capacity | Base discharge time | Base current | Base voltage | Base power | Base impedance |
|---|---|---|---|---|---|
| 45 A· h | 5 h | 9 A | 12 V | 108 W | 1.33 Ω |

Table 5.7: Base values for the Exide-Tudor battery studied

| Base capacity | Base discharge time | Base current | Base voltage | Base power | Base impedance |
|---|---|---|---|---|---|
| 65 A· h | 20 h | 3.25 A | 12 V | 39 W | 3.69 Ω |

Table 5.8: Base values for the BLA1 battery used by Doerffel

Comparing these two figures, there is apparently no relationship between them, as e.g., the discharged capacity and current are different, as Doerffel discharges its battery at 50 A and the Exide-Tudor battery is discharged at 138.42 A. However, if a per-unit system is defined and the same curves are compared in per unit values, other conclusions may be extracted. For both cases a set of base values are presented in Tables 5.7 and 5.8.

For these base values the same curves can be depicted as in Fig. 5.24, in which a simple comparison can be made. If the absolute value of both discharge currents are expressed as per-unit values, both batteries are then discharged with a 15.38 p.u. current. With the same per-unit current the Exide-Tudor battery presents a higher activation voltage drop, which is the voltage drop present at the beginning of the discharge. However, the Exide-Tudor discharges an 18 % less capacity than the battery of Doerffel, even though the battery used by Doerffel has nearly 31 % more rated capacity.

For example, the battery tested by Doerffel has a discharged capacity of 44.2 Ah, but this value does not give any information about the remaining capacity without an explicit reference to the rated capacity of the battery. On the other hand, 0.68 p.u. as the discharge capacity contains all the necessary information, as it is already referred to the rated capacity, once the set of base values are stated once and for all. Expressing all the results as p.u. values has an added value, as it allows a simple and direct comparison with similar work carried out by different authors, with different batteries, which can have very different characteristics (rated capacity, open circuit voltage, discharge time, etc).

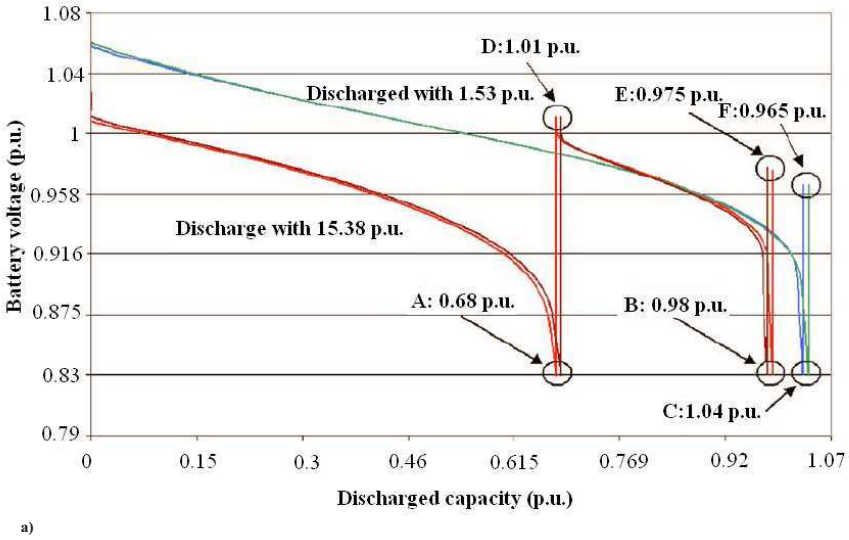


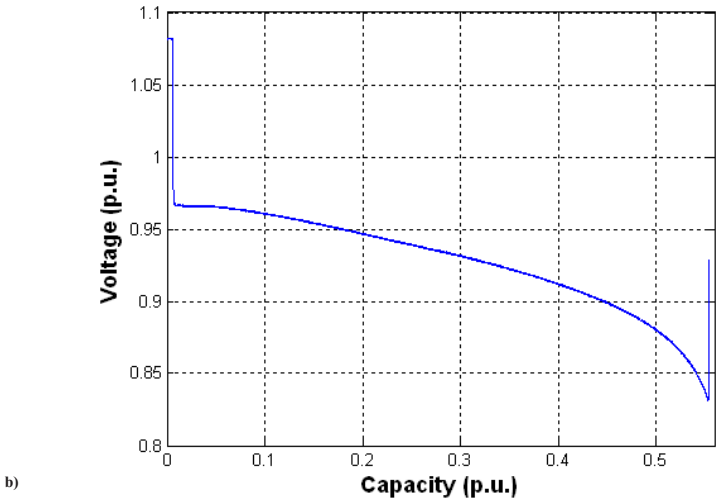


Fig. 5.24: Discharge curve obtained by a)Doerffel and b)Gauchia in p.u. values

### 5.6.3. Per-unit approach during alternate loads

The per-unit model and base magnitudes obtained in the previous section are especially useful for the interaction of the battery with other power systems also expressed in per-unit values. However, the dynamic behavior and internal processes of the battery include phenomena whose time horizon can be shorter than the 5 hours base time obtained previously. Hence, a more appropriate base system can be obtained to represent, study and compare

the internal electrochemical dynamic behavior of the battery.

This second temporal horizon is straightforward after conducting the EIS tests, as the most relevant phenomena takes place between 0.1 Hz and 6 kHz. For this frequency interval, the corresponding time range is 10 s and 0.16 ms, which is between three and seven orders of magnitude smaller than the 5 h discharge time horizon.

The dynamic time horizon is related to the frequency at which the dynamic processes occur. So a base frequency can be defined as a new base variable, which was not included in the previous base values due to the fact that these were defined for stationary values. However, the internal behavior of the battery is clearly dependant on the frequency, as reflected by the Nyquist plot. Hence, a criterion for the selection of the base frequency should be established. Studying the Nyquist plot, there are three singular candidate points to be considered. The first and second one are the cut-off frequencies for $R_1C_1$ and $R_2C_2$, defined as:

$$f_{c1} = \frac{1}{R_1 C_1} \qquad f_{c2} = \frac{1}{R_2 C_2} \tag{5.8}$$

The third possible point is the resonance frequency, defined as the frequency at which the capacitive and inductive impedances cancel each other, and therefore the battery impedance becomes purely resistive:

$$\begin{aligned} Z_{total}(\omega) = &\left[R_{ohm} + \frac{R_1}{1+\omega^2 C_1^2 R_1^2} + \frac{R_2}{1+\omega^2 C_2^2 R_2^2}\right] + ... \\ &... + j\omega \cdot \left[L - \frac{C_1 R_1^2}{1+\omega^2 C_1^2 R_1^2} - \frac{C_2 R_2^2}{1+\omega^2 C_2^2 R_2^2}\right] \end{aligned} \tag{5.9}$$

$$\mathrm{Re}\left[Z\left(\omega\right)\right]_{\omega=\omega_r} = R_{ohm} + \frac{R_1}{1+(2\pi f_r)^2 C_1^2 R_1^2} + \frac{R_2}{1+(2\pi f_r)^2 C_2^2 R_2^2} \tag{5.10}$$

The choice of the resonance frequency as the base frequency has a relevant advantage compared to the cut-off frequency, which is the simple identification in the Nyquist plot where $\mathrm{Im}[\mathrm{Z}(\omega)] = 0$, or in the Bode plot, where $\omega = 0$. As seen in Fig. 5.8, the resonance frequency is variable, as it decreases with increasing state of charge; therefore, one point of the curve must be selected as base frequency. Considering that the rest of base magnitudes

were selected for rated values and fully charged battery, it is logical to infer that the base frequency should also be selected for a fully charged battery. Therefore, the base frequency chosen for our Exide-Tudor battery is 189.87 Hz.

Known this base frequency, the frequencies magnitudes can be expressed in per-unit values for the rest of points of the EIS tests, if e.g. one point is at 400 Hz, its per-unit frequency would be 2.01 p.u. As it happened with the rest of per-unit magnitudes, knowing the per-unit frequency reveals more information than the absolute frequency. 2.01 p.u. means that the battery behavior is inductive, as the per-unit frequency is larger than 1 p.u., whilst 400 Hz does not give this information.

## 5.7. Conclusions

EIS tests were also applied to model the dynamic nonlinear behavior of batteries. A high number of tests were necessary due to the fact that batteries can present a wide range of states of charge, as well as accept an also wide range of currents. For both situations, charge and discharge processes were tested. However, time domain tests were also necessary to obtain the open circuit voltage hysteresis effect. This effect is rarely taken into account but can affect the resulting accuracy of model.

The direct comparison in absolute values of the equivalent circuit parameters renders confusing results due to the disparity of voltages and capacities. Therefore, in this Thesis we propose a per-unit system to correctly carry out this comparison, which, up to now, has not been found in literature. The per-unit system proposed includes, apart from the classical base voltage, current, power and impedance, a base time. Time is a key variable in batteries, due to the limited amount of reactants contained in the battery casing, and is related to capacity and current.

Batteries, as fuel cells, generate dc power. However, they can also accept, up to some extent, a certain amount of ac component superimposed on the dc current load. This ac current load frequency will influence the battery impedance behavior, and should therefore be taken into account. Through

the EIS tests carried out it is possible to know the capacitive, resistive and inductive behavior of the battery impedance. Therefore, for these ac component it is possible to define a base frequency. Various points were considered as possible base frequencies, but finally the resonance frequency was chosen. This choice was due to the resistive behavior at the resonance point (1 p.u.), which clearly identifies any capacitive (smaller than 1 p.u.) or inductive behavior (larger than 1 p.u.). Moreover, it is an easily identifiable point in both the Nyquist and Bode plots.

CHAPTER 6

# *Nonlinear dynamic model for ultracapacitors*

## 6.1. Introduction

This chapter presents a nonlinear dynamic model of ultracapacitors (also called supercapacitors) for simulation purposes. The model is experimentally validated under abrupt current loads.

The ultracapacitor modeled is a 3000 F 2.5 V Maxwell Boostcap. Its principal characteristics and photograph are shown in Table 6.1 and Fig. 6.1.

## 6.2. EIS tests experimental procedure

Ultracapacitors are receiving great attention by researchers, and due to its more recent development, the modeling techniques and model topology are still under investigation, as presented in the State-of-the-art, and there is not an unanimous equivalent circuit topology.

| | | |
|---|---|---|
| Capacitance | C (F) | 3000 |
| Maximum voltage | U (V) | 2.7 |
| DC series resistance | ESR dc (mΩ) | 0.29 |
| Series resistance at 1 kHz | ESR 1kHz (mΩ) | 0.24 |
| Leakage current | Ic (mA) | 5.2 |
| Shortcircuit current | Isc (A) | 4800 |
| Maximum specific energy | Emax (Wh/kg) | 5.52 |
| Maximum specific power | Pmax (W/kg) | 13.8 |
| Weight | m (kg) | 0.55 |

Table 6.1: Maxwell Boostcap 3000F ultracapacitor characteristics


Fig. 6.1: 3000F Maxwell ultracapacitor

Moreover, ultracapacitors are high power elements, which are capable of working with very high currents (hundreds of amperes) and which need special test conditions, which require equipments able to manage very high currents and small voltages.

Normally, impedance analyzers accept low currents (e.g. 60 mA) and medium voltages (45 V). This low maximum current forces the use of other equipments along with the impedance analyzer, such as potentiostats, which are able to absorb higher dc currents. Some examples are the 1287 A Solartron potentiostat, which endures up to 2 A, the Multi-Channel Cell Test System, also by Solartron, with a 5 A limit or the HCP-1005 Kromatec potentiostat which includes an 100 A booster.

The EIS tests can be carried out either with current control (galvanostatic mode) or with voltage control (potentiostatic mode). Either option requires an ac power source able to operate in a wide range of frequencies, at very high currents and low voltages. These conditions are very difficult to find in

conventional equipments (either potentiostats or power sources).

The current range is determined by the element under study. For very large capacitance values, such as those used in this work (3000 F 2.5 V) it can be easily deduced that current variations are as large as hundreds of amperes, which result in voltage variations of only some mV, the minimum value required to have a good signal-to-noise ratio. To carry out EIS tests under these conditions, the available commercial equipments were not useful. Therefore, in this Thesis we propose an experimental setup which allows to conduct frequency and time domain tests with high currents in a flexible and low cost way.

### 6.2.1. EIS test conditions

The first important decision which must be taken is under which mode the EIS tests should be carried out: galvanostatic or potentiostatic. To apply a potentiostatic (voltage control) EIS test it is necessary to use an ac power source, able to absorb high currents with low voltage and be able to work in a very wide range of frequencies. It is difficult to find an equipment which fulfills all these requirements. Therefore, the EIS tests are conducted in galvanostatic mode. Even if current is the control variable, the ultracapacitor voltage must be carefully monitored, to avoid over-voltage.

In order to define the range of current amplitudes to be used during the EIS tests, a series of previous measurements were made, starting at 20 A. In all cases the resulting voltage amplitudes were measured. It was found that, due to the very large capacitance of the ultracapacitor, the EIS results for ac currents below to 150 A were useless due to the insufficient ac voltage amplitude, which caused an incorrect impedance calculation. At 150 A, the EIS tests results were clear enough to ensure a correct measure, with an ac voltage amplitude of 70 mV.

The ac signal frequency is variable between 0.1 Hz and 1 kHz. The lower frequency limit is chosen due to the fact that smaller frequencies would lengthen the test duration and cause a significant variation of the test conditions.

The maximum frequency is limited to 1 kHz because the ultracapacitor inductive behavior is already clearly identified at this frequency.

For other electrochemical systems, such as batteries or fuel cells, the ac component is normally superimposed to a dc level. However, ultracapacitors charge and discharge very quickly and it is difficult to keep the test conditions in a narrow interval. For example, the discharge time can be as short as 30 s, with a voltage variation from 2.7 rated voltage to 0 V. EIS tests, taking into account the frequency range lasts 15 minutes, so an EIS tests during a dc discharge is not possible. Moreover, the tests conditions should be kept as constant and invariable as possible, so a variation of the 100 % of the test voltage is unacceptable. Therefore, the ac current will be the only current absorbed/supplied by the ultracapacitor. This test procedure guarantees that the voltage at the beginning and end of the test will be the same due to the fact that the energy stored during half of the period of the ac current signal will be discharged during the other half. The authors who have applied EIS to ultracapacitors did it in potentiostatic mode (voltage control). Only Buller [18] carried out a galvanostatic mode EIS, but did not describe the test procedure.

In order to obtain an equivalent circuit, the dependency of the parameters of the equivalent model with current and/or voltage should be investigated. As explained in [21], [20] or [17], and unlike batteries or fuel cells, ultracapacitors parameters depend on the voltage, instead of the current, so the charge stored depends on the capacitance and voltage.

Taking into account the preceding considerations, the ultracapacitor will be tested under the following conditions:

- DC current: 0 A.
- AC current amplitude: 150 A.
- DC voltage: 1.5 V, 2 V and 2.5 V.
- Frequency: 0.1 Hz to 1 kHz.

### 6.2.2. EIS experimental setup proposed

To carry out the EIS tests, the equipment used is the following:

- Impedance analyzer: Solartron 1260.
- DC Electronic load: Chroma 63201 (60 V, 300 A).
- DC Power source: Sorensen 20-150E (12 V, 150 A).
- dSpace PX 10. The signals are acquired through an input/output board DS 2201, which is connected to its connector panel CP 2201. Both elements are part of a dSpace real-time control and acquisition system. The I/O DS 2201 board has 20 input channels, with 5 A/D converters which multiplex 4 channels each. There are 8 output channels with 8 parallel D/A converters. All the channels have a 12 bit resolution.
- LEM transducer: LA-205 S.
- Computer.

The EIS test is controlled by the impedance analyzer, which is the equipment which varies the frequency and monitors current and voltage to calculate the impedance. Due to the fact that it cannot directly generate a 150 A ac signal, the impedance analyzer controls other equipments which can work at high currents: the dc electronic load and power source. As explained in Figs. 6.2 and 6.3, the impedance analyzer is programmed to generate an ac voltage signal, which is monitored by the dSpace system. Through Matlab/Simulink, this signal is separated in its positive and negative semi-cycles. The positive semi-cycle is scaled to control the electronic load, which will sink the corresponding ac current. Meanwhile, the negative semi-cycle is scaled to program the dc power source, which will supply the corresponding ac current. Therefore, the coordinated and real-time control of the electronic load and power source results in a constant amplitude/variable frequency current at the ultracapacitor terminals, which follows the control signal generated by the impedance analyzer.

According to the wiring diagram depicted in Fig. 6.4, the ultracapacitor is connected in parallel to the electronic load and power source. In this way, it can absorb the current during positive semi-cycles and release it during

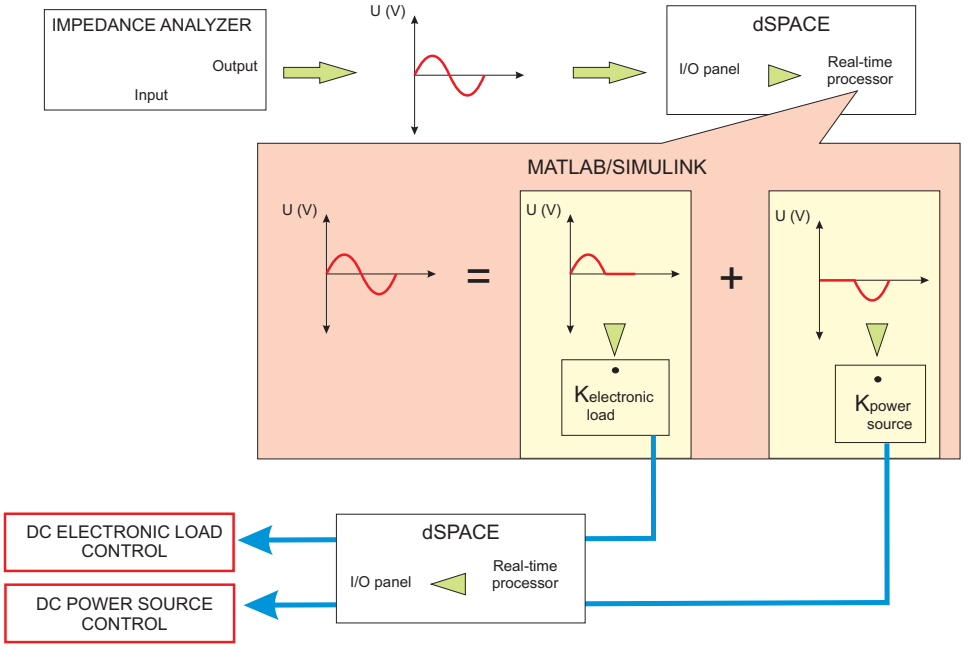


Fig. 6.2: EIS control procedure for ultracapacitors

negative semi-cycles. A current LEM transducer is connected in series with the ultracapacitor to measure the current, which is sent to the impedance analyzer. The voltage at terminals of the ultracapacitor is directly sent to the impedance analyzer, which accepts dc voltages smaller to 42 V. With the current and voltage measures the impedance analyzer is able to calculate the ultracapacitor complex impedance. The laboratory setup diagram and photograph are shown in Figs. 6.4 and 6.5.

### 6.2.3. EIS tests results

The graphical representation of the EIS tests are the Nyquist plots shown in Fig. 6.6. The ultracapacitor capacitive behavior is restricted to a small interval (from 0.1 Hz to 31.6 Hz). For the lower frequencies of this interval the Nyquist plot is practically a vertical line, which is the representation of a capacitance in series with a resistance, whose value (0.25 mΩ) is identified as the intersection between the curve and the abscissa axis. In literature, this part of the curve is not totally vertical due to the contact resistance between components, high electrode porosity or low proton mobility inside the electrodes [95].

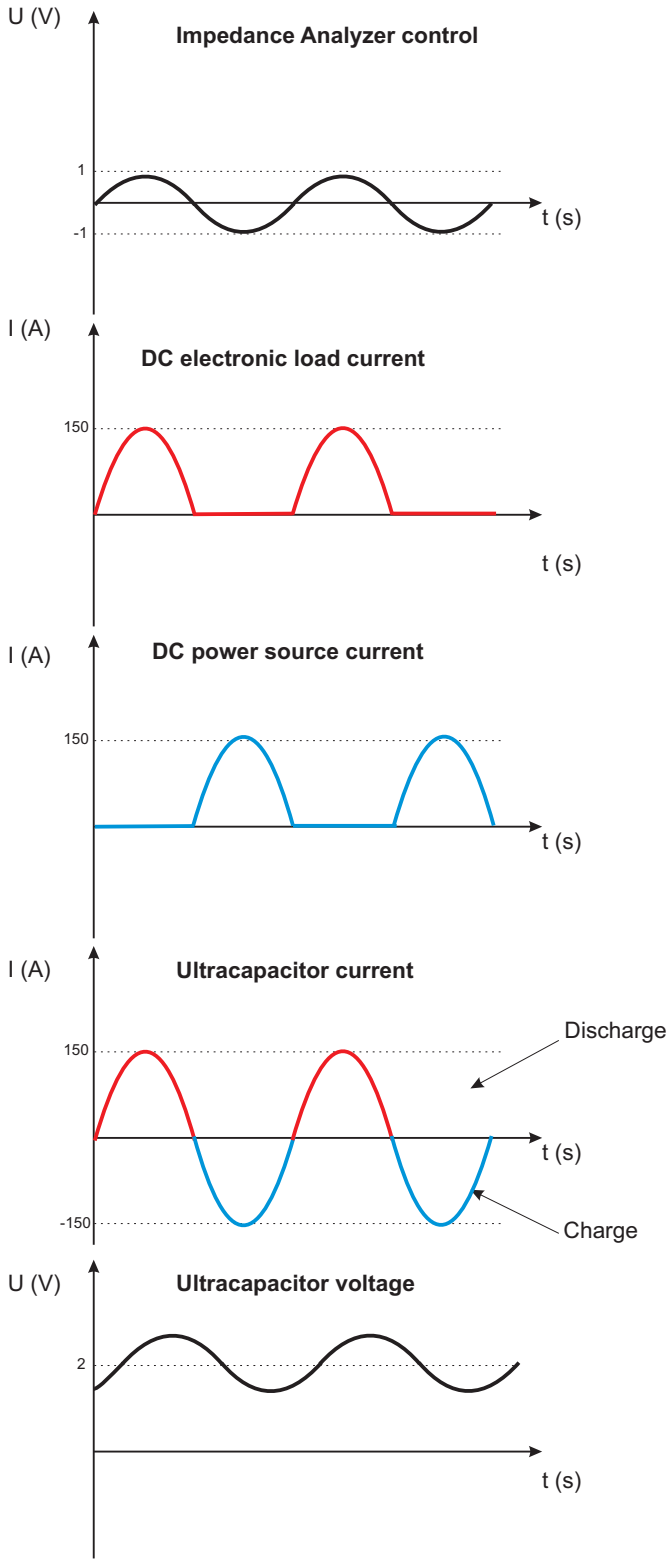


Fig. 6.3: Currents and voltage evolutions for each equipment

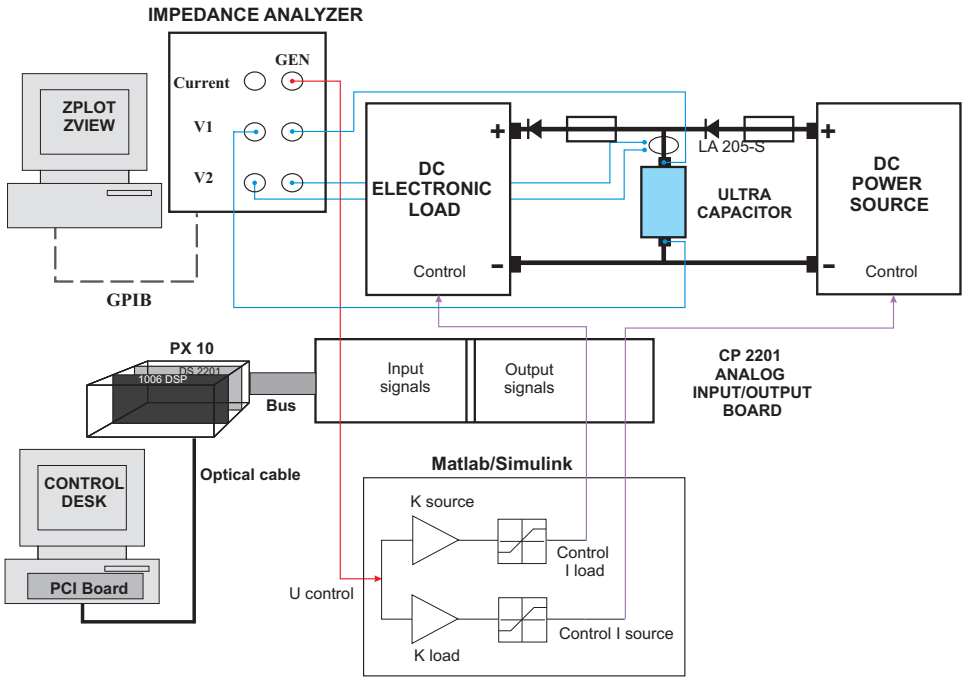


Fig. 6.4: EIS experimental setup

From 1 Hz to 31.6 Hz the complex impedance changes to a 45º slope due to diffusion phenomena at the electrode pores. In literature, some authors such as Barsoukov [46] and Brouji [76] explain that the ultracapacitor electrodes are highly porous structures, through which the charge transport resembles a transmission power electric line, due to the fact that the pore diameter is small compared to its length. This diffusion phenomena can be represented by a Warburg impedance, which is the series connection of RC networks. In this Thesis, the diffusion has been represented with two RC networks, avoiding the use of higher number of networks, which complicate the modeling and require more computational work.

From 31.6 Hz onwards, the ultracapacitor behavior is totally inductive. In literature, most authors neglect or do not comment the ultracapacitor inductive behavior and do not present this region on the Nyquist plot. Other authors such as [18], just mentions it, whilst [21] or [20] state that during inductive behavior the real part of the impedance increases due to skin effect. However, our results show that the real part of the impedance decreases before it starts increasing. At these frequencies, the current does not flow

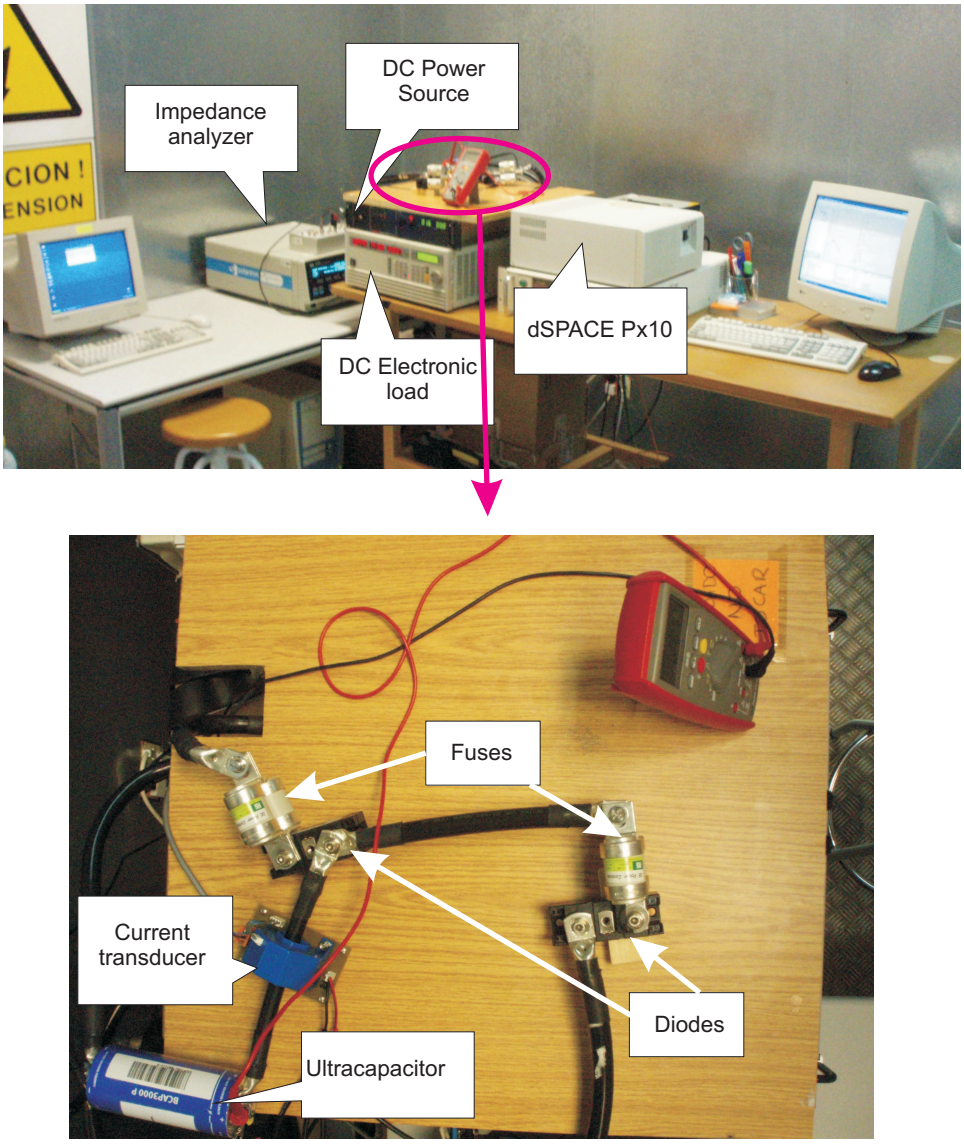


Fig. 6.5: Photograph of the ultracapacitor EIS setup

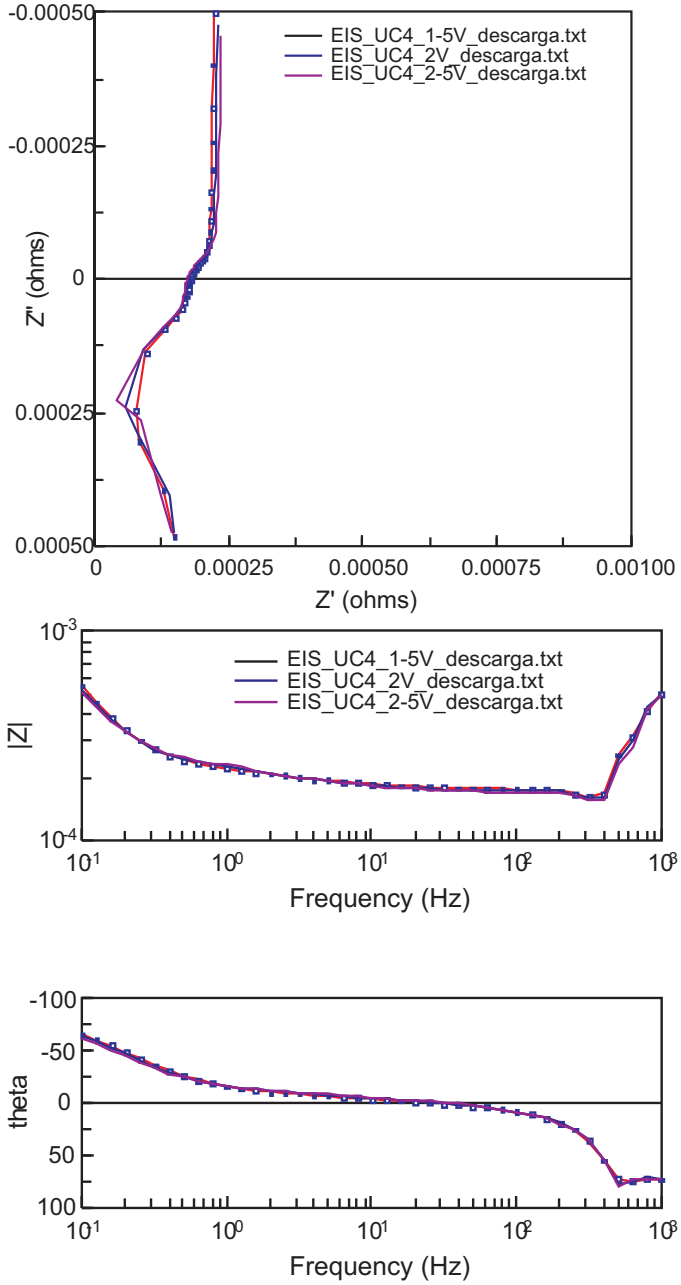


Fig. 6.6: Nyquist and Bode plots obtained for the ultracapacitor after the EIS tests

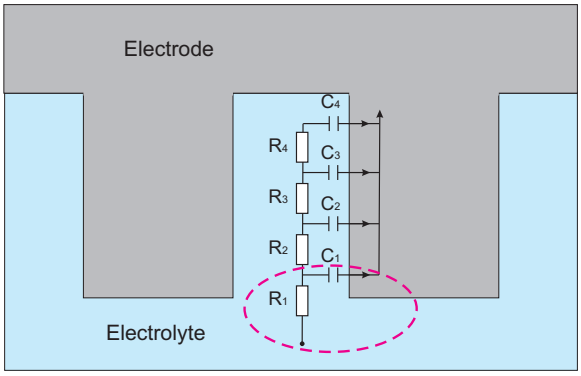


Fig. 6.7: High frequency effect on the pore effective surface. Adapted from [29]

inside the pores, but stays at the beginning of the pore, as depicted in Fig. 6.7. This implies that most of the current flows through the bulk material, whose resistance is smaller than the electrolyte resistance, causing the reduction seen in the Nyquist plot. When the frequency increases this effect is summed up with the skin effect, which causes an eventual increase of the real part of the impedance. The real part of the impedance should be always positive, therefore, possible negative values are due to small errors present when the real part of the resistance is $10^{-4}$ Ω.

Among the wide variety of equivalent circuits under study, the best fit of the Nyqist plot was found for the circuit structure shown in Fig. 6.8. The parameters obtained present assumable errors, and only one parameter presents an error bigger than 10 %. The values obtained from ZView were introduced in the software Statgraphics, in order to obtain the polynomial dependency of each parameter with the voltage. The model obtained explains the 100 % of the variability. The equations obtained are shown in (6.1).

$$
\begin{aligned}
&\mathrm{L\ (H)} = 1.15 \cdot 10^{-7} - 7.10 \cdot 10^{-9} \cdot \mathrm{U} + 8.80 \cdot 10^{-10} \cdot \mathrm{U}^2 \\
&\mathrm{C}_1(F) = 1816 + 1260 \cdot \mathrm{U} - 244 \cdot \mathrm{U}^2 \\
&\mathrm{C}_2\ (\mathrm{F}) = 2307 - 648 \cdot \mathrm{U} + 100 \cdot \mathrm{U}^2 \\
&R_2(\Omega) = 1{,}16 \cdot 10^{-5} + 2{,}09 \cdot 10^{-5} \cdot U - 0{,}19 \cdot 10^{-5} \cdot U^2 \\
&C_3\ (\mathrm{F}) = 1.51 + 1.11 \cdot \mathrm{U} - 0.29 \cdot \mathrm{U}^2 \\
&R_3(\Omega) = 6{,}39 \cdot 10^{-4} - 1{,}47 \cdot 10^{-4} \cdot U + 0{,}36 \cdot 10^{-4} \cdot U^2
\end{aligned}
\tag{6.1}
$$

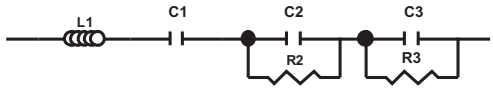


| Element | Freedom | Value | Error | Error % |
|---|---|---|---|---|
| L1 | Free(+) | 1,0728E-7 | 1,5885E-9 | 1,4807 |
| C1 | Free(+) | 3157 | 75,692 | 2,3976 |
| C2 | Free(+) | 1560 | 319,51 | 20,481 |
| R2 | Free(+) | 3,8784E-5 | 3,9544E-6 | 10,196 |
| C3 | Free(+) | 2,532 | 0,099294 | 3,9216 |
| R3 | Free(+) | 0,00016681 | 2,193E-6 | 1,3147 |

| | |
|---|---|
| Chi-Squared: | 0,01661 |
| Weighted Sum of Squares: | 1,2624 |
| Data File: | D:\SANDRA\RESULTADOS EIS UC\Definitivos\EIS |
| Circuit Model File: | D:\SANDRA\RESULTADOS EIS UC\Circuito Equival |
| Mode: | Run Fitting / Freq. Range (0,1 - 1000) |
| Maximum Iterations: | 800 |
| Optimization Iterations: | 0 |
| Type of Fitting: | Complex |
| Type of Weighting: | Calc-Modulus |

Fig. 6.8: Equivalent circuit fitted with ZView

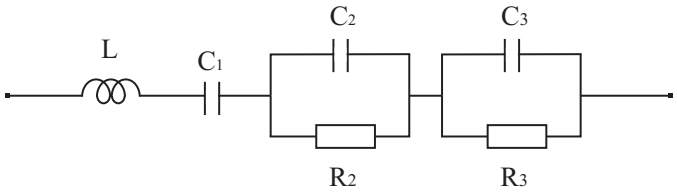


Fig. 6.9: Ultracapacitor equivalent circuit

### 6.2.4. Ultracapacitor impedance model and validation

With the previous equations, the model obtained is shown in Fig. 6.9. It can be observed that, unlike batteries or fuel cells, the ultracapacitor model is a purely passive model, with no voltage or current sources. All the elements involved present electrical equations, which are easily programmed in Matlab/Simulink. The voltage at the ultracapacitors terminal programmed corresponds to 6.2.

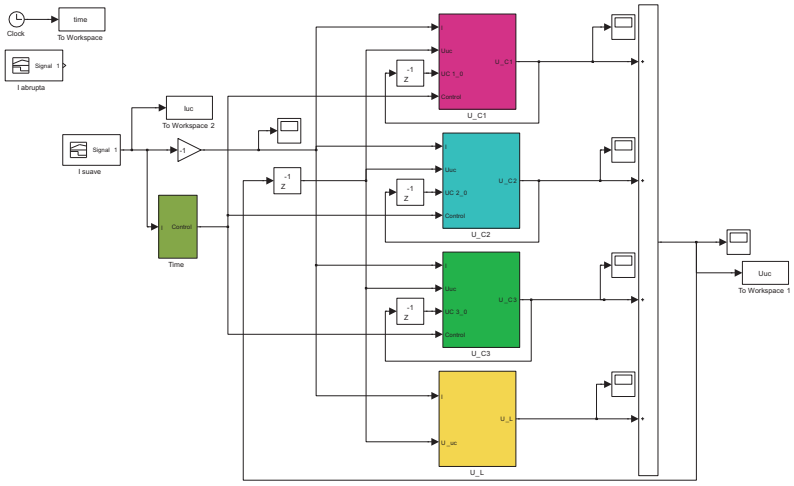


Fig. 6.10: Ultracapacitor Matlab/Simulink model

$$
\begin{aligned}
U_{uc} &= U_L + U_{C_1} + U_{C_2} + U_{C_3} \\
U_L &= L \cdot \frac{dI}{dt} \\
U_{C_1} &= \int \frac{1}{C_1} \cdot I \cdot dt \\
U_{C_2} &= \int \frac{1}{C_2} \cdot \left( I - \frac{U_{C_2}}{R_2} \right) \cdot dt \\
U_{C_3} &= \int \frac{1}{C_3} \cdot \left( I - \frac{U_{C_3}}{R_3} \right) \cdot dt
\end{aligned}
\tag{6.2}
$$

The ultracapacitor model has two inputs and one output. The inputs are the current demanded and the voltage at its terminals. This ultracapacitor models needs an initial voltage value to begin the simulation. The model output is the voltage at the terminals of the ultracapacitor. The Matlab/Simulink model is shown in Fig. 6.10

To obtain an experimental validation of the model, an abrupt load current profile, depicted in Fig. 6.11, was programmed and the voltage at terminals monitored. The experimental and modeled voltages are compared in Fig. 6.12. It can be observed that the ultracapacitor time constant is very small and causes the dynamic evolution to present a linear evolution under abrupt

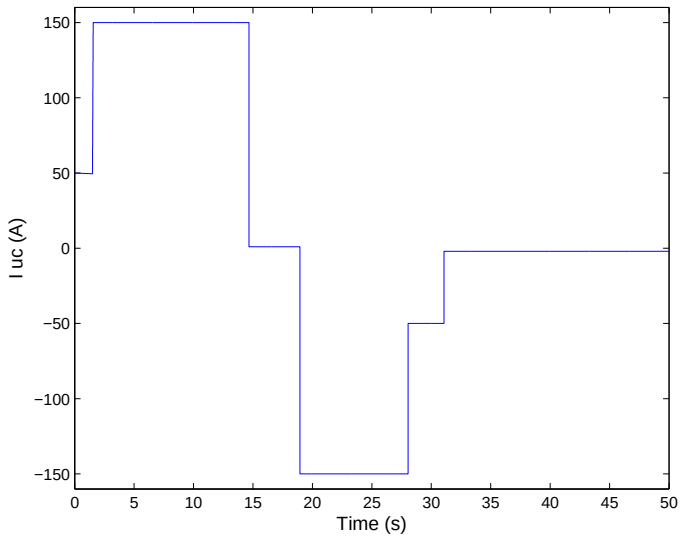


Fig. 6.11: Abrupt ultracapacitor current load

current profiles. The model follows quite precisely the experimental voltage.

## 6.3. Conclusions

Ultracapacitors are a relatively new technology, and therefore, its test procedure, equivalent circuit and characteristic curve are not universally defined. Moreover, ultracapacitors are high power elements which need special test considerations. These considerations are rarely mentioned in literature, where authors avoid disclosing its test setup and procedure, and most of them do not make any attempt to validate the model proposed.

Ultracapacitors tested up to now are usually smaller than the 3000 F ultracapacitor tested in this Thesis. Therefore, the equipments used by other authors, frequently not mentioned, are not applicable due to its small current limit. In this Thesis we propose an EIS test procedure which allows to carry out these test during the high currents needed to obtain a correct impedance calculation. The setup proposed uses conventional laboratory equipments, such as dc electronic load and dc power source, which can be synchronously controlled by an impedance analyzer through a real-time acquisition and control system.